Received: 22 July 2017 | Revised: 22 May 2018 | Accepted: 4 June 2018

DOI: 10.1111/gbi.12304

ORIGINAL ARTICLE

WILEY gebiology

Snapshot of an early Paleoproterozoic ecosystem: Two diverse microfossil communities from the Turee Creek Group, Western Australia

Erica Victoria Barlow[1,2] | **Martin Julian Van Kranendonk**[1,2,3]

[1]Australian Centre for Astrobiology, School of Biological, Earth and Environmental Sciences, University of New South Wales, Kensington, New South Wales, Australia

[2]Australian Research Council Centre of Excellence for Core to Crust Fluid Systems (CCFS), Macquarie University, Sydney, New South Wales, Australia

[3]Big Questions Institute, University of New South Wales, Kensington, New South Wales, Australia

Correspondence
Erica Victoria Barlow, Australian Centre for Astrobiology, School of Biological, Earth and Environmental Sciences, University of New South Wales, Kensington, NSW 2052, Australia.
Email: evbarlow@gmail.com

Abstract

Eighteen microfossil morphotypes from two distinct facies of black chert from a deep-water setting of the c. 2.4 Ga Turee Creek Group, Western Australia, are reported here. A primarily *in situ*, deep-water benthic community preserved in nodular black chert occurs as a tangled network of a variety of long filamentous microfossils, unicells of one size distribution and fine filamentous rosettes, together with relatively large spherical aggregates of cells interpreted as in-fallen, likely planktonic, forms. Bedded black cherts, in contrast, preserve microfossils primarily within, but also between, rounded clasts of organic material that are coated by thin, convoluted carbonaceous films interpreted as preserved extracellular polymeric substance (EPS). Microfossils preserved within the clasts include a wide range of unicells, both much smaller and larger than those in the nodular black chert, along with relatively short, often degraded filaments, four types of star-shaped rosettes and umbrella-like rosettes. Large, complexly branching filamentous microfossils are found between the clasts. The grainstone clasts in the bedded black chert are interpreted as transported from shallower water, and the contained microfossils thus likely represent a phototrophic community. Combined, the two black chert facies provide a snapshot of a microbial ecosystem spanning shallow to deeper-water environments, and an insight into the diversity of life present during the rise in atmospheric oxygen. The preserved microfossils include two new, distinct morphologies previously unknown from the geological record, as well as a number of microfossils from the bedded black chert that are morphologically similar to—but 400–500 Ma older than—type specimens from the c. 1.88 Ga Gunflint Iron Formation. Thus, the Turee Creek Group microfossil assemblage creates a substantial reference point in the sparse fossil record of the earliest Paleoproterozoic and demonstrates that microbial life diversified quite rapidly after the end of the Archean.

KEYWORDS

community, ecosystem, Great Oxidation Event, Gunflint microbiota, microfossil, Turee Creek Group

1 | INTRODUCTION

Archean sedimentary rock successions preserve only relatively simple microfossils including filamentous, unicellular and spindle-shaped microfossils that are often found only in isolated, single populations (e.g., Czaja, Beukes, & Osterhout, 2016; Klein, Beukes, & Schopf, 1987; Knoll & Barghoorn, 1977; Kremer & Kazmierczak, 2017; Lanier, 1986; Sugitani, Grey, Nagaoka, Mimura, & Walter, 2009; Sugitani, Mimura, Nagaoka, Lepot, & Takeuchi, 2013; Sugitani, Mimura, Takeuchi, Lepot, et al., 2015; Sugitani, Mimura, Takeuchi, Yamaguchi, et al., 2015; Wacey, Kilburn, Saunders, Cliff, & Brasier, 2011; Walsh, 1992; amongst others). It is not until the c. 1.88 Ga Gunflint Iron Formation, Canada, that a variety of microbial forms with more complex morphologies are preserved, such as *Kakabekia*, *Eoastrion* and *Eosphaera* (Barghoorn & Tyler, 1965). In contrast, Meso- and Neo-Proterozoic rocks contain many diverse examples of microfossils with complex morphology, often preserved alongside other microfossils in communities. Examples include the following: *Tappania plana* from the ≥1.4 Ga Ruyang Group, China (Lan et al., 2014; Yin, 1997; Yin, Xunlai, Fanwei, & Jie, 2005), c. 800–900 Ma Wynniatt Formation, Canada (Butterfield, 2005a, b) and c. 1.5 Ga Roper Group Australia (Javaux & Knoll, 2016); *Shuiyousphaeridium macroreticulatum*, also from the Ruyang Group (Yin, 1997); *Bangiomorpha pubescens* from the c. 1.2 Ga Hunting Formation, Canada (Butterfield, 2001; Butterfield, Knoll, & Swett, 1990); and *Bonniea dacruchares* and other vase-shaped microfossils from the c. 750 Ma Chuar Group, USA (Porter, Meisterfeld, & Knoll, 2003). However, the early Paleoproterozoic fossil record surrounding the c. 2.45–2.32 Ga Great Oxidation Event (GOE; Bekker et al., 2004; Farquhar, Bao, & Thiemens, 2000; Holland, 2002) is particularly sparse.

Microfossils have recently been reported from black chert in the c. 2.45–2.21 Ga Turee Creek Group, Western Australia, by Schopf et al. (2015) and Fadel, Lepot, Busigny, Addad, and Troadec (2017). Both studies described similar tangled, cobweb-like masses of filamentous microfossils, but proposed different metabolic interpretations: a sulfur-cycling biocoenose (Schopf et al., 2015) and an iron-oxidising community (Fadel et al., 2017). Here, we build on this previous work by presenting a comprehensive description of a diverse assemblage of newly discovered microfossils from different outcrops of the same unit as previously described, including a number of forms not previously reported from rocks of this age. These include microfossils from two distinct communities, permineralised in two distinctly different black chert facies; nodular and bedded. Both of these black chert facies occur within a few metres stratigraphic height of one another, and both within deeper-water facies, offshore from a shallow-water dolomitic stromatolite–thrombolite reef complex (Barlow, Van Kranendonk, Yamaguchi, Ikehara, & Lepland, 2016). A benthic, deeper-water community with possible infallen planktonic forms is preserved in the nodular black chert facies, whilst the bedded black chert facies preserves a shallower water, likely phototrophic community in organic clasts that were transported into the deeper-water setting. Eighteen distinct microfossil morphotypes, as well as films interpreted as preserved extracellular polymeric substance (EPS), are described, including two forms that are new to the geological record. Part of the Turee Creek microfossil assemblage described here from the bedded black cherts is morphologically similar to, yet 400–500 Ma older than, type specimens from the c. 1.88 Ga Gunflint Iron Formation (Barghoorn & Tyler, 1965; Fralick, Davis, & Kissin, 2002) and is 100–300 Ma older than the slightly older Gunflint correlatives (e.g., the c. 2.1 Ga Franceville Group in Gabon; Amard & Bertrand-Sarfati, 1997; Lekele Baghekema et al., 2017). Combined, the nodular and bedded black chert facies described here provide insight into an early Paleoproterozoic ecosystem at the time when life was adapting to the rise of atmospheric oxygen.

1.1 | Geological setting

The Turee Creek Group (TCG) consists of, from base to top, the Kungarra, Koolbye and Kazput formations (Thorne & Tyler, 1996; Thorne, Tyler, & Blight, 1995; Trendall, 1979). The TCG lies conformably on the Boolgeeda Iron Formation of the older Hamersley Group and is unconformably overlain by the Beasley River Quartzite of the Wyloo Group. The minimum age of the TCG is 2,209 ± 15 Ma, as determined from SHRIMP U-Pb dating of zircons in the Cheela Springs Basalt that overlies the Beasley River Quartzite (Martin, Li, Nemchin, & Powell, 1998). A maximum age of the TCG is 2,449 ± 3 Ma; the age of the Woongarra Rhyolite that conformably underlies the Boolgeeda Iron Formation (Barley, Pickard, & Sylvester, 1997). Krapez, Müller, Fletcher, and Rasmussen (2017) reasoned that the TCG may have been deposited much earlier, between 2,445–2,420 Ma, based on detrital zircon geochronology and estimated sedimentation rates. In addition, the Meteorite Bore Member, which sits within the Kungarra Formation of the TCG, is interpreted to have been deposited towards the end of the GOE (Williford, Van Kranendonk, Ushikubo, Kozdon, & Valley, 2011). Combined, it is likely that the majority of the TCG was deposited across the rise of atmospheric oxygen, c. 2.4 Ga.

This study is focused on black chert units that reside in the deeper-water part of a stratigraphic succession that conformable overlies a shallow-water dolomitic stromatolite-thrombolite reef complex from the TCG. This succession lies to the north-west of the Hardey Syncline, near the old Duck Creek Homestead. The ~350 m (true thickness) shallow-water reef complex and conformably overlying deeper-water succession crops out for ~15 km along strike on the eastern limb of a tight, faulted, north-west-plunging syncline that was labelled the "Kazput Syncline" by Barlow et al. (2016) (Figure 1). The TCG dolostone unit at this locality strikes NW-SE and dips, on average, 37° to the SW (Barlow et al., 2016; Martin, Powell, & George, 2000; Van Kranendonk, 2010). Relatively shallow-water stromatolites and thrombolites at the base pass through dolomitic turbidites into deeper-water, thinly bedded dolosiltite, shale and thinly bedded ironstone with black chert nodules, followed by thinly bedded dolosiltite with thin beds of black chert (see figure 20 of Barlow et al., 2016). The shale and ironstone

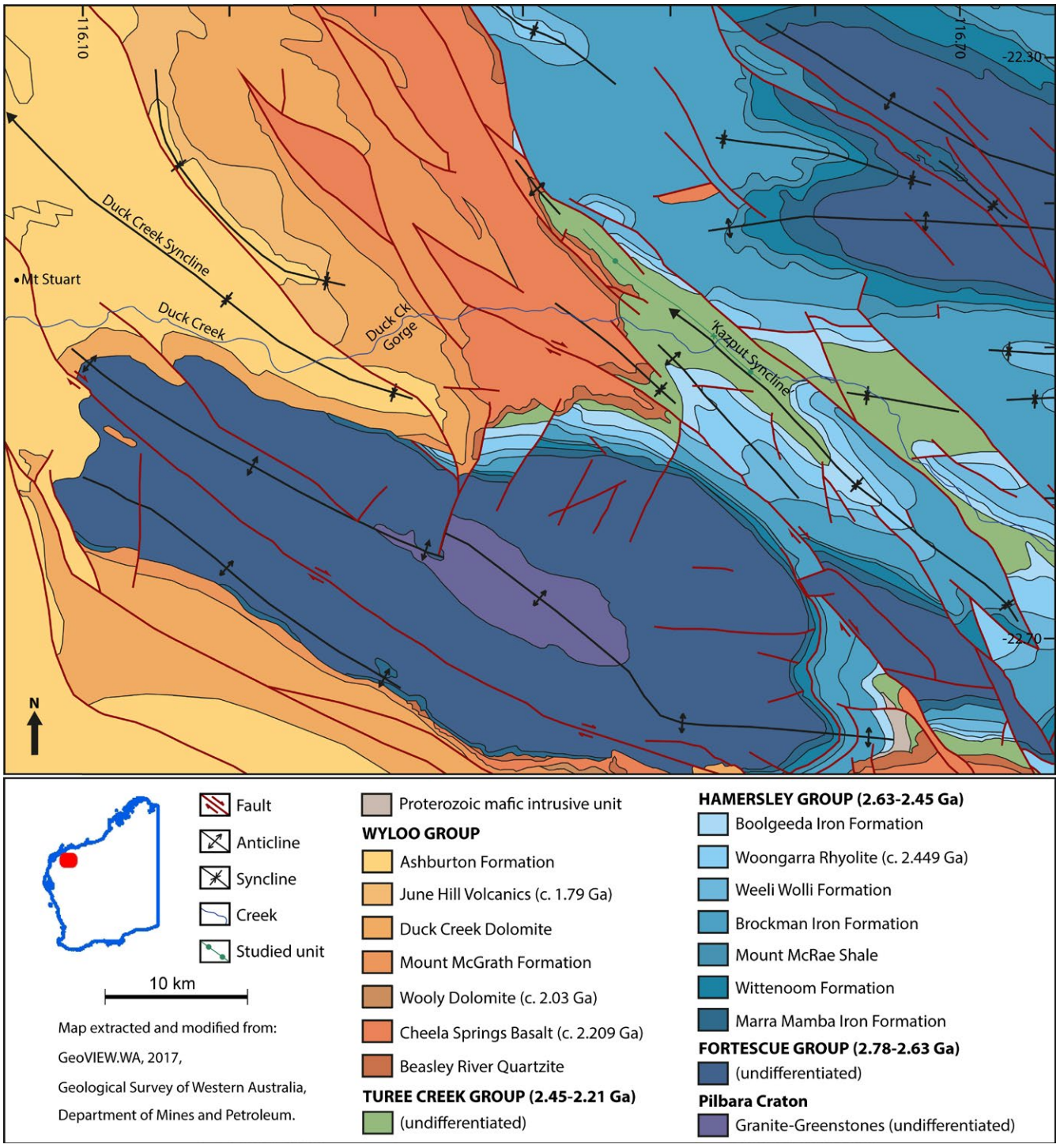

FIGURE 1 Geological map showing the location of the studied unit on the eastern limb of the "Kazput Syncline" within rocks of the Turee Creek Group, which conformably overlie the Boolgeeda Iron Formation of the Hamersley Group. Note the tightly folded, north-west-plunging "Kazput Syncline" is unconformably overlain by the open and continuous Duck Creek Syncline (for further detail regarding the unconformities in this area, please refer to figures 1 and 2 of Barlow et al., 2016). The area along the green line was mapped in this study and designates the extent of the stromatolitic dolomite ridge (labelled "studied unit"). The extent along strike of the deeper-water nodular and bedded black chert units is represented by the area between the two green circles along this line, with the locality of Fadel et al. (2017) shown by a green cross [Colour figure can be viewed at wileyonlinelibrary.com]

units were interpreted by Barlow et al. (2016) as the deepest point in the exposed succession (end of a transgression), with the return to thinly bedded dolosiltite with interlayers of bedded black chert signifying the beginning of a regression. Overlying units are cut off by a fault that follows the axial plane of the "Kazput Syncline" (see figure 2 of Barlow et al., 2016).

The "Kazput Syncline" is a tight, north-west-plunging fold structure that is part of an older generation of folds and faults that predate the younger, and much larger, Duck Creek Syncline (DCS), whose axial plane lies ~25 km further to the west (Figure 1; Barlow et al., 2016; Geological Survey of Western Australia, 2017; Martin & Morris, 2010; Van Kranendonk, 2010). The DCS is a large (~20 km half wavelength), open, north-west-plunging fold structure that contains the major outcrops of the younger, c. 1.8 Ga Duck Creek Dolomite, including the well-studied Duck Creek Gorge locality (Figure 1; Grey, 1985; Grey & Thorne, 1985; Knoll & Barghoorn, 1976; Knoll, Strother, & Rossi, 1988; Schopf et al., 2015; Walter, 1972; Wilson et al., 2010).

Barlow et al. (2016) interpreted the dolomitic stromatolite-thrombolite reef complex to be part of the Kazput Formation, based on mapping that identified an immediately underlying unit of quartz-rich sandstone that they correlated with the Koolbye Formation in the Hardey Syncline further to the south-east. Instead, Krapez et al. (2017) classified the stromatolitic dolomite ridge as part of the underlying Kungarra Formation. Despite these different interpretations of the specific formation, the important point is that all researchers agree that the studied unit belongs to the TCG (e.g., Barlow et al., 2016; Fadel et al., 2017; Hickman & Van Kranendonk, 2012; Krapez, 1996, 1999; Krapez et al., 2017; Martin, 1999; Martin & Morris, 2010; Martin et al., 2000; Powell & Horwitz, 1994; Simonson, Schubel, & Hassler, 1993; Trendall, Compston, Nelson, De Laeter, & Bennett, 2004; Van Kranendonk, 2010; Van Kranendonk, Mazumder, Yamaguchi, Yamada, & Ikehara, 2015; Williford et al., 2011). As we have no further evidence to directly support either interpretation, we simply refer to the succession studied here as belonging to the Turee Creek Group.

2 | TUREE CREEK GROUP MICROFOSSILS

2.1 | Previous work

Microfossils were first reported from the TCG dolomite ridge locality (north-west of the Hardey Syncline) by Van Kranendonk et al. (2012), who described four types of filamentous microfossils of varying width, including two with apparent beaded-cells, tangled together in cobweb-like masses surrounding clear domains of quartz. Van Kranendonk et al. (2012) noted that some filaments were exceptionally long (hundreds to thousands of micrometres in length) and posited their origin as possibly sulfur-cycling based on their position within deeper-water sediments, as well as morphological similarity to modern sulfur-cycling micro-organisms.

Following on from this initial discovery, Schopf et al. (2015) reported three varieties of filamentous microfossils from a locality ~65 km to the south-east (lat. 22.48°S, long. 116.52°E) of the c. 1.8 Ga Duck Creek Dolomite. These filamentous microfossils range in size from relatively large (~7–9 μm diameter) filaments with possible 12–15 μm long elongated cells, to thinner (~1–4 μm diameter) filaments with possible bead-shaped cells, to very narrow (≤1 μm diameter) thread-like filaments, and are interlaced together in a wispy, cobweb-like fabric (Schopf et al., 2015). Schopf et al. (2015) interpreted these three filamentous forms, along with other morphologically similar filaments from the younger Duck Creek Dolomite, as representing the remains of a deep-water sulfuretum community, on the basis of the deep-water settings, morphological comparison of the microfossils with modern sulfur-cycling organisms, and results from sulfur isotope analyses of inferred microbial pyrite in the Duck Creek Dolomite samples ($\delta^{34}S$ values ranged from −9.4 to +43.4‰).

Similar filamentous microfossils also preserved in tangled, cobweb-like masses were reported by Fadel et al. (2017) from the same dolomite ridge as this current study, but from a slightly different locality (at 22°29.748′S, 116°31.817′E). Fadel et al. (2017) identified four filamentous forms: "type 1" narrow filaments, 2–3 μm in diameter, with a thin continuous sheath (30–100 nm thick); "type 2" narrow filaments with thin central tubes (1–1.5 μm in diameter), bound by thick granular sheaths (3.5–5 μm wide) and light and dark banding along their length; "type 3" broad filaments, 3–10 μm in diameter, with thin discontinuous sheaths (50–100 nm thick); and "type 4" siderite-rich, highly degraded filaments with poorly preserved granular kerogen. Fadel et al. (2017) interpreted that the iron present in these samples, in the form of siderite, ankerite and minor Fe-silicates, was originally a product of the metabolisms of Fe-oxidising micro-organisms. Similarly, Wilson et al. (2010) suggested an iron-based metabolism for microfossils preserved within cherts in ironstone from the c. 1.8 Ga Duck Creek Dolomite.

2.2 | New microfossil locality

The microfossil-containing nodular black chert and bedded black chert facies described here from the TCG dolomite ridge locality were mapped for ~12.5 km along strike. Hundreds of samples of nodular and bedded black chert were collected between 22°26.291′S, 116°27.888′E and 22°31.021′S, 116°33.151′E (see green circles in Figure 1), including at the collection site of Fadel et al. (2017). The stratigraphy of 10 transects across the deeper-water units is summarised in Figure 2a.

Nodular black chert occurs over a ~2 m thick section of interbedded, finely laminated iron-rich shale and fine-grained bedded dolosiltite, which overlies a ~0.5–1 m thick unit of fissile grey-weathering shale (Figure 2a,c–e). In some places, nodular chert in ferruginous deposits also occurs immediately stratigraphically below the shale, but this is not always exposed. The black chert nodules are ~20 cm wide by ~7 cm high, on average, but range to both smaller and larger sizes. Bedding is commonly bent around the base of black chert nodules (Figure 2d), but in some rare cases, both the base of a nodule and the underlying bedding are flat. The contact of the chert nodules with the interbedded shale and dolosiltite layers is wrinkly on a millimetre scale (arrow, Figure 2d). On fresh surfaces of hand samples, the internal texture of the nodules is uniform, cryptocrystalline and very dark blue-black, with no trace of internal bedding.

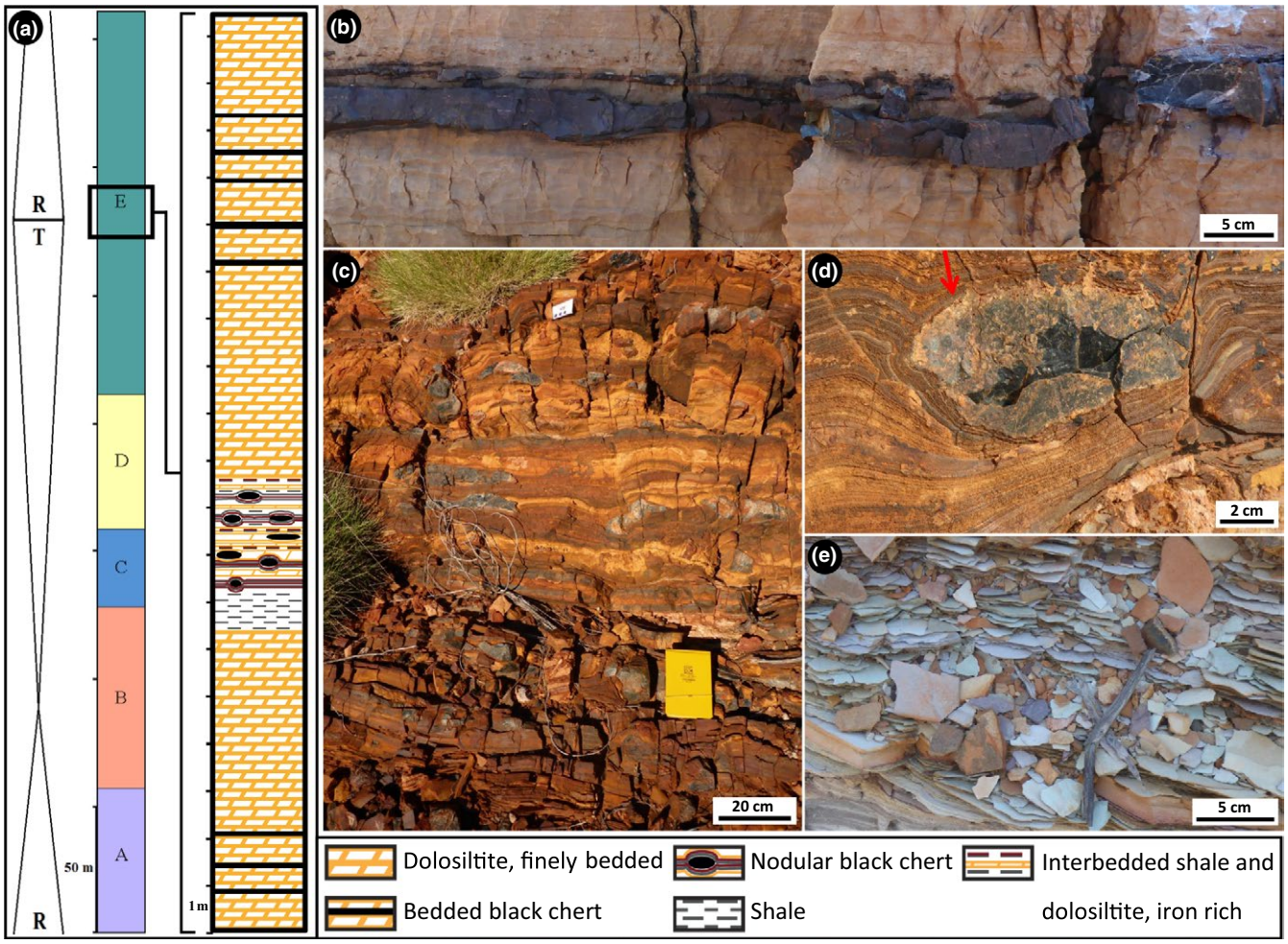

FIGURE 2 (a) Middle and left-hand side columns: summary of facies relationships from Barlow et al. (2016) showing regression (R) and transgression (T) sequences. Assemblages A–D represent the stromatolite–thrombolite reef, which transitions to deeper-water units in Assemblage E (see Barlow et al., 2016 for detail). Right-hand side: representative stratigraphic column across the deeper-water section of stratigraphy summarised from transects of the deeper-water units in this study, including the bedded black chert units, the shale and the interbedded shale and ironstone unit containing nodules of black chert. In some places, nodular chert in ferruginous deposits also occurs immediately stratigraphically below the shale, but this is not always exposed. (b) Outcrop photograph of bedded black chert and thinly bedded dolosiltite. Right-hand side shows location of hand sample, within which most of the images in Figures 8 and 9 were taken. (c) Outcrop of interbedded shale–ironstone–nodular black chert. (d) Close-up of black chert nodule highlighting the layers bending around underneath the nodule, indicating silicification precompaction. Contact of chert nodule with surrounding layers is wrinkly on a millimetre scale (arrow). (e) Fissile, grey-weathering shale that underlies the interbedded shale–ironstone–nodular black chert sequence in (c) [Colour figure can be viewed at wileyonlinelibrary.com]

Bedded black chert units occur over a stratigraphic thickness of ~4 m, interbedded with thinly bedded dolosiltite, and are present both underneath and overlying the shale–ironstone–nodular chert sequence (Figure 2a). Bedded black chert beds are each 2–4 cm thick (Figure 2b), reaching a maximum of 6 cm thick, and are spaced every 40–100 cm apart. Individual beds extend for 10's of metres along strike before pinching out, and then reappearing.

Distinct, separate communities of well-preserved microfossils are permineralised within the nodular and bedded black chert units. Nodular black chert contains a wide variety of microfossil morphologies, including five long filamentous forms of various thicknesses; unicells; fine filamentous rosettes; and relatively large (~80–138 μm), spherical aggregates of cells. In contrast, bedded black chert contains microfossils that are preserved both within and between rounded carbonaceous clasts. These clasts are ~200–1,000 μm in diameter and loosely packed in a grainstone with a silicified matrix of mosaic microquartz. Many of the grainstone clasts are coated by undulating to convolute carbonaceous films, interpreted as preserved EPS. Microfossils preserved inside the grainstone clasts include three distinct sizes of unicells; short, often degraded filamentous microfossils; four types of star-shaped rosettes; and umbrella-like rosettes. Large, complexly branching filamentous microfossils were observed in between the grainstone clasts.

Overall, 18 microfossil morphotypes, as well as films interpreted as preserved EPS, are described from within black chert from the TCG ridge (Table 1), including two new morphologies previously unknown from the literature.

TABLE 1 Summary of the 18 morphotypes of Turee Creek Group microfossils reported here. Eight are from the nodular black chert unit and ten from the bedded black chert unit. In addition, kerogenous films in the bedded black chert are interpreted as preserved extracellular polymeric substances (EPS)

Morphotypes	Width	Length	Cell diameter	Figure no. (context)	Figure no. (microscale)
NODULAR BLACK CHERT					
Filament type 1	10–14 μm	>250 μm	No visible cells	3a–d; S4	4a
Filament type 2	5–9 μm	~700 μm	Potential cells: ~12 μm long alternating dark (carbonaceous-rich) and light (carbonaceous-poor) bands	3a–d; S4	4b
Filament type 3	1.4–3 μm	~200 μm	No visible cells	3a–d; S4	S1A,B
Filament type 4	0.5–1.2 μm	100's of μm	No visible cells	3a–d; S4	4a–d; S1B
Filament type 5	3–4 μm	575 μm	Smooth sheaths: no visible cells	5a	5b–d; S1C
Unicell type 1	20 μm	20 μm	~20 μm	3a–d; 4e; S4	4f; S1B
Fine filamentous rosette	Individual filaments: ~0.4 μm	20–30 μm	No visible cells	6a–c	6d,e; S1D
	Rosettes: 35–50 μm	NA	No visible cells		
Spherical aggregate*	80–138 μm	NA	10–25 μm	7a,c	7b,d–f; S1E
BEDDED BLACK CHERT					
Unicell type 2	3–17 μm	NA	3–17 μm	8a–e; 10a	8g,h,j; S2B
Unicell type 3 (internal organic masses)	12–19 μm	NA	12–19 μm	8a–e; 10a	8f,h
Unicell type 4	>30–47 μm	NA	>30–47 μm	8a–e; 10a	8i
Filament type 6	1–2.5 μm	50–100 μm	4–9 μm long segments, possibly elongated cells	8a–e; 10a	8c,d,j; S2C
Star-shaped rosette type 1 (asterisk-like)	Individual filaments: ≤1.5 μm	10 μm	No visible cells	8a–e; 10a	9a
	Rosettes: avg. 20–25 μm	NA	No visible cells		
Star-shaped rosette type 2 (sinuous filaments)	Individual filaments: <1 μm	≥10 μm	No visible cells	8a–e; 10a	9b,c
	Rosettes: avg. 25 μm	NA	No visible cells		
Star-shaped rosette type 3 (large opaque central core, short tapering filaments)	Individual filaments: <1 μm	5–8 μm	No visible cells	8a–e; 10a	9d,e
	Rosettes: avg. 25 μm	NA	No visible cells		
Star-shaped rosette type 4 (small opaque central core, long straight filaments)	Individual filaments: <1 μm	~15 μm	No visible cells	8a–e; 10a	9f; S3A
	Rosettes: avg. 35 μm	NA	No visible cells		
Umbrella-like rosette	Mantle: ~37 × 55 μm diameter	NA	No visible cells	8a–e; 10a	9g; S3B
Large, complexly branching filamentous rosette*	Individual filaments: ~1–3 μm	35–55 μm	No visible cells	8a,b; 10a	9h–j; S3C
	Rosettes: 75–100 μm	NA	No visible cells		
Film coating grainstone clasts	~2 μm thick	NA	No visible cells	8a,b; 10a–c	10d,e; S3D

Note. The two forms marked by an asterisk* (spherical aggregates and large, complexly branching filamentous rosettes) are defined here as new microfossils, previously unknown from the geological literature.

2.3 | Nodular black chert

Nodules of black chert typically occur dispersed irregularly throughout the unit of interbedded shale, ironstone and dolosiltite (Figure 2c). There are three clear types of internal textures that are present within separate samples of nodular black chert from this unit, and different microfossils are associated with each. The first texture most commonly found within nodular black chert samples is that previously described by Schopf et al. (2015) and Fadel et al. (2017), of relatively long filamentous microfossils of different length and diameter, tangled in a web-like network surrounding ellipsoidal to partly polygonal domains that now consist of coarse mosaic to spherulitic microquartz (Figure 3). We observed an absence of pyrite within this texture. The outlines of the clear domains appear, in some areas, to resemble crystal shapes, and the microquartz fill becomes coarser towards the centres of these domains. The second texture within separate samples of nodular black chert is that of "rivers" of straw-like filaments (different to those filaments in the web-like fabric above), surrounding circular patches of microquartz that contain framboidal pyrite (Figure 5a). These first two textures have minimal trace of bedding at micrometre scale. In contrast, the third type of texture observed within nodular black chert samples is that of well-defined layers that consist of dense clumps of organic matter that are elongated along bedding planes, along with abundant, small organic clots. Minimal pyrite is observed in texture 3, except within the more degraded samples. This third type of nodular chert sample preserves spherical aggregate microfossils, described below, which are unknown from the geological record and are presented here as a new form.

2.3.1 | Long filamentous microfossils

At least four different filamentous microfossil types are recognised within the tangled network (texture 1) described above: (1) thick filaments, 10–14 μm wide and >250 μm long (Figure 4a); (2) 5–9 μm wide and ~700 μm long filaments with alternating, ~12 μm long dark (carbonaceous-rich) and light (carbonaceous-poor) bands (Figure 4b); (3) 1.4–3 μm wide and ~200 μm long filaments (Figure S1A,B); and (4) thin, thread-like filaments, 0.5–1.2 μm wide and 100's of micrometres long (Figure 4c,d).

In one thin section cut perpendicular to bedding, 150–350 μm long filamentous microfossils are oriented parallel to one another and aligned vertically relative to bedding (Figure 4e). These filaments are overlain by a ~50 μm thick layer of more densely packed horizontal filaments that are aligned parallel relative to bedding (arrows, Figure 4e). This vertical-horizontal arrangement is repeated in multiple areas throughout the sample (arrows in Figure 3a), in some cases up to three tiers at a time, across a thickness of ~1,500 μm (Figure S4). This vertical-horizontal arrangement is interpreted as a preserved life array, with the filamentous micro-organisms in original growth position.

A fifth filamentous form observed in other samples of nodular black chert (texture 2) is characterised by hollow, straw-like filaments, 3–4 μm wide and up to 575 μm long (Figure 5). This form does not occur within the tangled filamentous networks in Figures 3 and 4, described above, but is commonly preserved in aligned "rivers" of filaments encircling patches of microquartz that contain central clusters of framboidal pyrite grains (Figure 5a). More rarely, these filaments are bent (Figure 5b). The lack of observed cell remains in any of these straw-like filaments could indicate that they were dead for a longer period before being silicified, compared to filament type 2 described above (Figure 4b), and, as a result, lost the internal cell detail. These straw-like filaments could be the external sheaths of filamentous bacteria, as sheaths are more resistant to decomposition than the cells they once housed (Bartley, 1996).

Petrographic observations show that the alignment and orientation of both the filaments in the tangled networks and the straw-like filaments appear to be unaffected by the growth of silica crystals in the matrix, as the filaments are observed to be continuous, straight through silica grain boundaries (Figures 4c,d and 5c,d). This is true of even the smallest (~1 μm diameter), thread-like filamentous microfossils (Figure 4c,d). Indeed, silica crystals are often observed growing off filamentous microfossils, in towards the centres of the clear microquartz spaces (Figure 3d). This supports the notion by Fadel et al. (2017) that silica crystallisation was not responsible for the development of the tangled network pattern, but that this represents a primary texture of the community structure.

2.3.2 | Unicellular microfossils

Within the tangled network of filamentous microfossils (nodular black chert texture 1) are type 1 unicells, ~20 μm in diameter (arrows, Figure 4F). These single spherical cells are generally uniform in size and appear to be filled by organic matter, rather than hollow as in the case of unicellular microfossils from the bedded black chert described below. The dense unicells are spaced throughout the tangled filamentous microfossil network and occur as isolated cells, not in aggregates. They are particularly well developed in the vertically oriented array of filaments shown in Figure 4E.

2.3.3 | Fine filamentous rosettes

Fine filamentous rosettes consist of extremely thin, short filamentous microstructures, ~0.4 μm wide and 20–30 μm long, which radiate out from a single point (Figure 6). In general, these thin filaments are straight, but in some examples, they are slightly wavy along their length (e.g., red arrows, Figure 6d). The radiating rosettes are composed of kerogen (Figure S1D), are sometimes asymmetric, and vary in overall diameter from ~35 to 50 μm depending on the number of thin filamentous microstructures clumped together. The rosettes are generally preserved in radial, fibrous quartz, yet do not appear to be the nucleation site of silica spherulites (Figure 6b,e). The fine filamentous rosettes are observed both within samples containing the larger, tangled filamentous microfossils (i.e., nodular black chert texture 1), and those containing the spherical aggregate microfossils (texture 3).

2.3.4 | Spherical aggregate microfossils

Relatively large spherical aggregate microfossils (~80–138 μm in diameter) are observed within nodular black chert texture 3. These

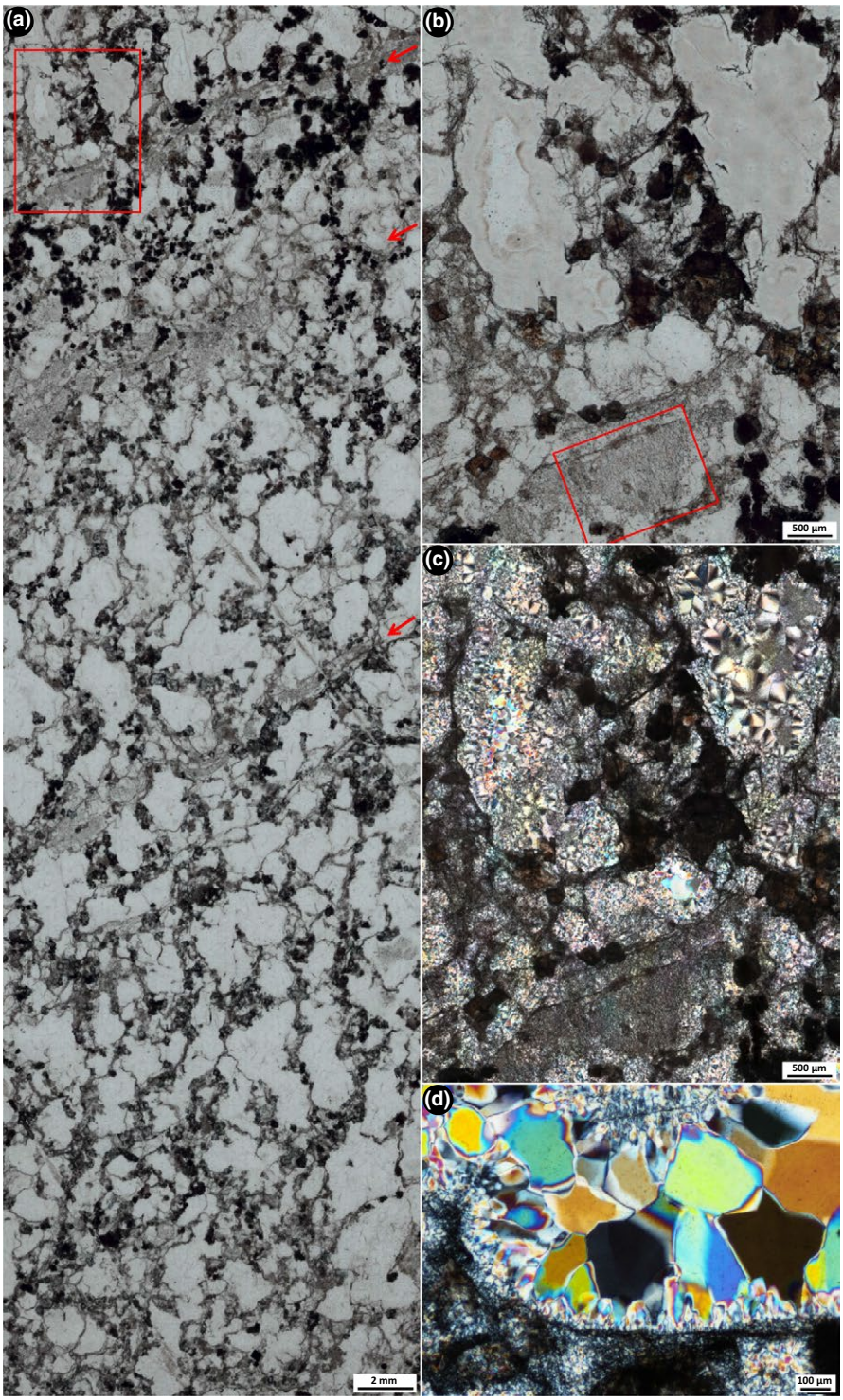

FIGURE 3 Nodular black chert texture 1, showing the tangled microfossil network. (a) Large stitched image of the tangled network of filamentous microfossils and unicells separating clear ellipsoidal domains of quartz. Note the faint, spaced layers (arrows) in which the filamentous life arrays are preserved (box shows location of b–c). (b) Close-up of (a) (box shows location of Figure 4e). (c) Same view as (b), under cross polars, showing that finer-grained quartz rims the clear domains and coarsens inwards, with some centres chalcedonic (top right of image). (d) Edge of tangled filamentous network surrounding a clear ellipsoidal domain, under cross polars. Microcrystalline quartz crystals appear to initially grow from the tangled network out towards the centre of the clear domain, which consists of macrocrystalline quartz crystals, showing that quartz growth did not cause the tangled network texture [Colour figure can be viewed at wileyonlinelibrary.com]

microfossils consist of densely packed aggregates of smaller cells (~10–25 µm in diameter) that create a honeycomb-like network of organic matter (Figure 7). These microfossils have a distinctive rind, or halo, which is free of the fluffy organic material that is distributed throughout the rest of the sample (e.g., see Figure 7d; Figure S1E). Very fine-grained microquartz occurs within, and in the halo immediately around, the spherical aggregates. This microquartz is significantly finer than that which fills the surrounding area and is apparent in examples where spherical aggregates are cut thin by the section (Figure 7a–c). Protruding into the fine-grained, kerogen-free halo are irregularly shaped, thin kerogenous structures that extend out from the main spherical body (arrows, Figure 7e,f).

With changing focal depth under the microscope, it is clear that the aggregates are spherical in shape. They range in size, at least in part, depending on where the thin section surface intersects the spherical aggregate or the individual cells; that is, if the microfossil is

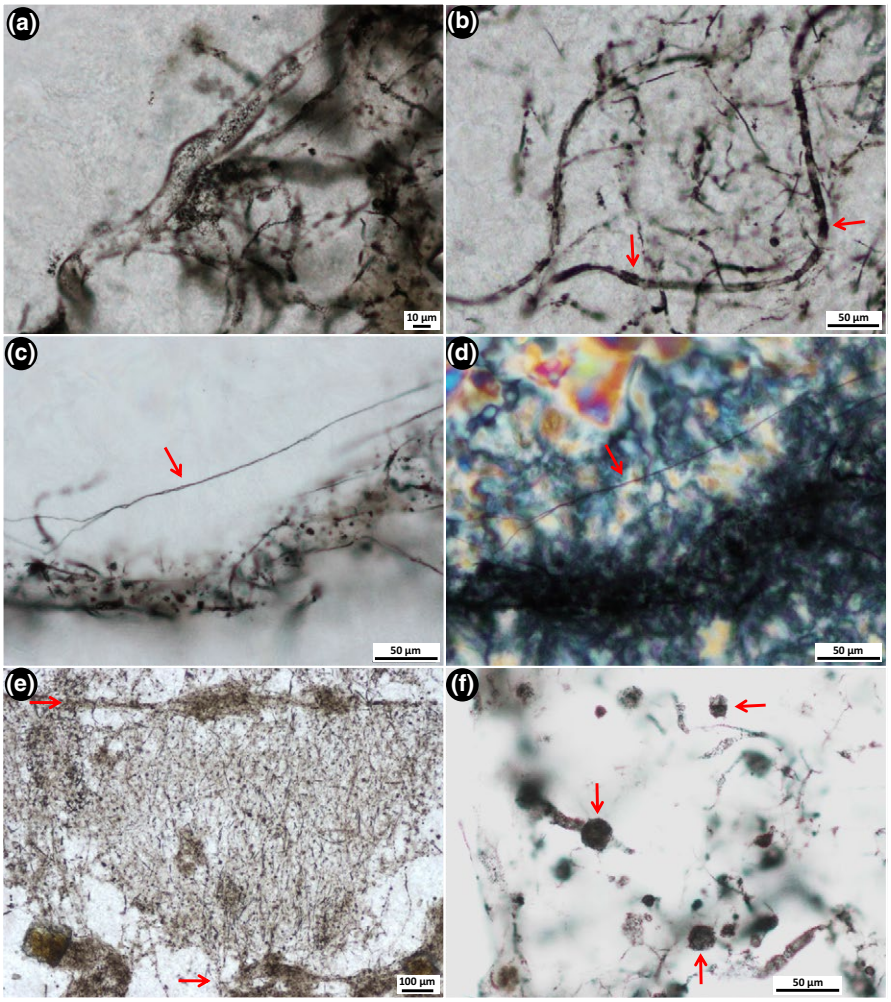

FIGURE 4 Microfossils within the tangled network of nodular black chert texture 1. (a) Large filamentous microfossil 10–14 µm wide (type 1). Parts of filament types 3 and 4 are also in focus. (b) Dense, tangled filamentous microfossil network, displaying filament types 2–4. Note the prominent dark (carbonaceous-rich) and light (carbonaceous-poor) banding along the length of filament type 2 (arrows). (c) Two thin, thread-like filamentous microfossils (type 4) twisted around one another (arrows). (d) Same view as (c), under cross polars, showing that the orientation and shape of these filaments appear to be independent of silica crystal growth. (e) A unique arrangement of filaments preserved in life array: the bulk of the image contains vertically aligned filaments, bracketed with horizontally aligned filaments (arrows) above and below. (f) Arrows highlight type 1 unicellular microfossils (image overexposed to view unicells more clearly amongst the tangled filaments) [Colour figure can be viewed at wileyonlinelibrary.com]

sliced closer to the bottom of the sphere, the width will appear smaller than if sliced directly through the middle. This also affects the opacity of the spherical aggregate; it is denser when sliced near the top or in the centre of the microfossil, as opposed to across the bottom.

2.4 | Bedded black chert

Bedded black chert beds are, on average, 2–4 cm thick, but can be up to 6 cm thick and are interbedded with thinly bedded dolosiltite. Chert beds are most often black, but are also sometimes grey-coloured. They occur every 40–100 cm up-section and continue for 10's of metres along strike, before pinching out, then reappearing. In thin section, the bedded black cherts are composed of well-rounded, elongate to spherical and sometimes cuspate-shaped clasts consisting of kerogenous material and microfossils (Figures 8 and 10). The kerogenous clasts range in size from ~200 to 1,000 µm in diameter and contain a regular distribution of organic material throughout (Figure 8c–e; Figure S2A), lacking any evidence of either concentric layering or a central nucleus, as in ooids (Boggs, 2009). The clasts consist of kerogen in fine-grained microquartz that is significantly finer-grained than the coarser, mosaic microquartz that fills the matrix between the clasts (Figure 8b). Carbonate rhombs (~80–120 µm in size) show growth zoning, are generally ferruginous, and occur exclusively within the kerogenous clasts. Thin, commonly highly ornate, kerogenous films (~2 µm thick) coat the outside of most kerogenous grainstone clasts (Figure 10).

Nine microfossil morphologies are recognised *within* the grainstone clasts. These include three distinct types of unicells, short filamentous microfossils, four distinct morphologies of star-shaped rosettes, and umbrella-like rosettes. The star-shaped rosettes and umbrella-like rosettes are similar to, but 400–500 Ma older than, type specimens of *Eoastrion* and *Kakabekia umbellata*, respectively, from the c. 1.88 Ga Gunflint Iron Formation (Awramik & Barghoorn, 1977; Barghoorn & Tyler, 1965; Cloud, 1976). A tenth microfossil morphotype that consists of large, complexly branching filamentous rosettes was found *in between* the clasts, and is considered here to represent a new type of microfossil, previously undescribed from the literature.

2.4.1 | Unicellular microfossils

Well-preserved unicells are abundant within the grainstone clasts (Figure 8c–j), much more so than those in the nodular black chert microfossil assemblage. These unicells from within clasts are generally perfectly spherical, with well-defined cell walls, and have been divided into three categories based on size (unicell types 2–4:

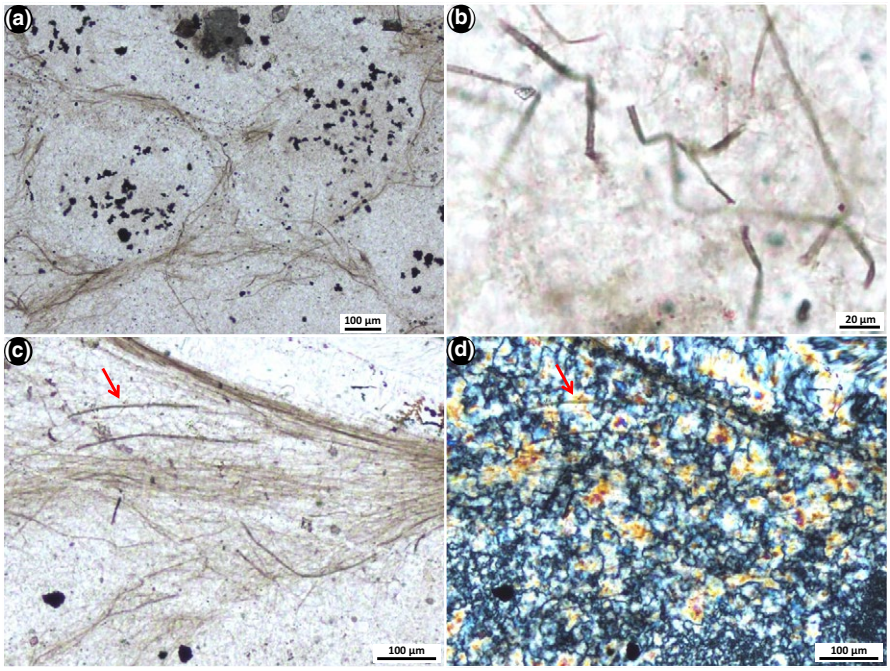

FIGURE 5 Hollow, straw-like filamentous microfossils (type 5), within nodular black chert texture 2. (a) "Rivers" of filaments encircle patches of finer-grained silica with central clusters of framboidal pyrite grains (black crystals). (b) In rare cases, straw-like filaments are sharply bent. (c, d) Thick "rivers" of straw-like filaments (d under cross polars). Arrows point to the same microfossil, highlighting that the orientation and shape of these filaments appear to be independent of mesoquartz grain boundaries; their alignment is irrespective of crystal growth [Colour figure can be viewed at wileyonlinelibrary.com]

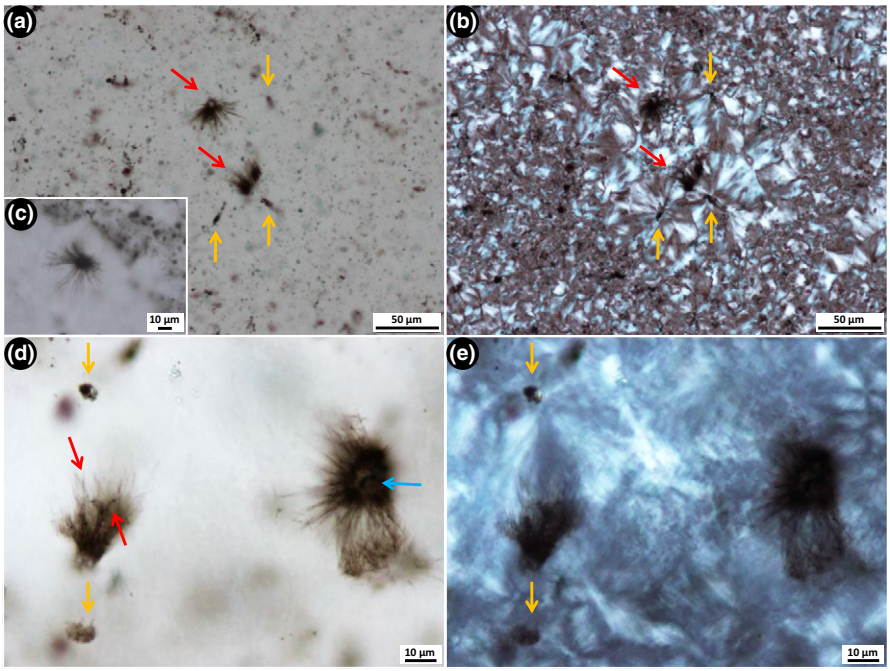

FIGURE 6 (a) Fine filamentous rosettes within the nodular black chert comprise extremely thin, short filamentous microstructures (red arrows). Orange arrows indicate non-filamentous kerogenous clots. (b) Same view as (a), under cross polars, showing the rosettes are preserved within radial, fibrous quartz. Note that the clots of kerogen directly beside the rosettes are also within radial, fibrous quartz, but are not elongated into filamentous shapes (orange arrows). (c) Fine filamentous rosette within nodular black chert. Note lack of outer "rim," like in similar-looking forms reported in Tyler and Barghoorn (1954). (d) Close-up of rosettes: red arrows point to curved filaments, and blue arrow highlights a central point from which the thin filamentous microstructures radiate. Orange arrows show non-filamentous clots of kerogen. (e) Same view as (d), under cross polars. Orange arrows indicate kerogenous clots that, despite also being preserved within fibrous quartz, do not have a filamentous form [Colour figure can be viewed at wileyonlinelibrary.com]

Table 1). Type 2 unicells (Figure 8g–j) range from ~3 to ~17 µm in diameter and resemble *Huroniospora* Barghoorn from the Gunflint Iron Formation (Barghoorn & Tyler, 1965). One example of a possible dividing cell was observed, in which two oval-shaped unicells share a straight cell wall (septum?), and appear to be encased in a circular outer wall (Figure 8g). Type 3 unicells are slightly larger (up to ~19 µm

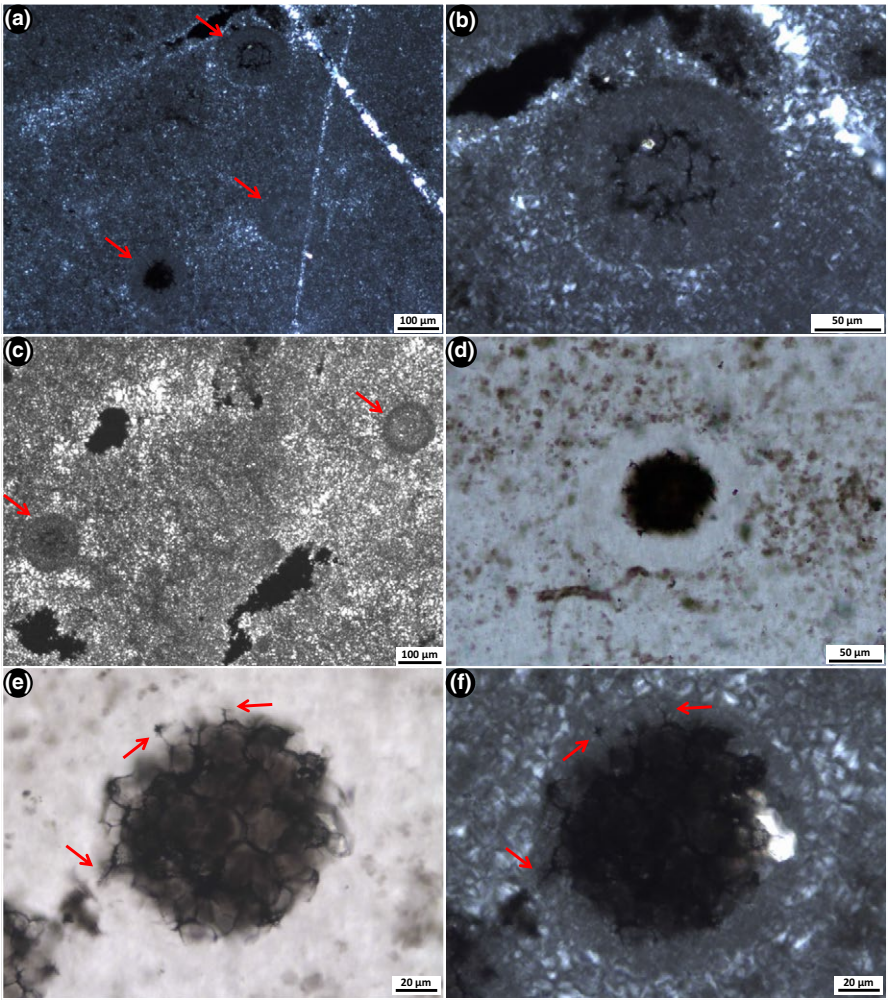

FIGURE 7 Spherical aggregate microfossils within nodular black chert texture 3. (a–c) Spherical aggregates are preserved within finer quartz than the surrounding matrix and appear less dense when they are cut by the thin section (arrows show location of aggregates). (b) shows a close-up of the topmost spherical aggregate in (a). (d) Each spherical aggregate has a kerogen-free halo evenly surrounding it. (e) Cells that make up the aggregate are ~10–25 µm in diameter, and are made clearer by the dark, kerogenous outlines which give this microfossil a characteristic honeycomb-like appearance. Arrows point to irregularly shaped, thin kerogenous structures extending out from the main body. (f) Same view as (e), under cross polars, highlighting the rind of extremely fine-grained microquartz that surrounds these microfossils. The bright pale yellow on the right-hand edge is a dolomite crystal underneath the fossil, within the thickness of the slide [Colour figure can be viewed at wileyonlinelibrary.com]

in diameter) and contain an internal dark brown spherical mass (Figure 8f,h), which could be remnant of an internal organic structure (Oehler, 1976a). This type of unicell is similar to *Leptoteichos golubicii* described by Knoll, Barghoorn, and Awramik (1978). In contrast, type 4 unicells are much larger, ranging from >30 to 47 µm in diameter, and do not appear to contain internal masses (Figure 8i). Although unicell types 2–4 are observed in close association with one another, they generally appear only as single, individual cells rather than as closely packed colonies.

2.4.2 | Filamentous microfossils

Filamentous microfossils are present inside many of the grainstone clasts (type 6; Figure 8c,d,j). These microfossils are, on average, ~1–2.5 µm wide and ~50–100 µm long. They are much darker, shorter and more dispersed than any of the tangled and straw-like filamentous microfossils in the nodular chert. In rare cases, filamentous microfossils from the grainstone clasts are segmented in fragments, 4–9 µm long (arrow in Figure 8j), but in most cases—and unlike the well-preserved unicells within the clasts—these filamentous microfossils are degraded, with diffuse and patchy outlines (arrows in Figure 8c).

2.4.3 | Star-shaped rosettes

A range of star-shaped rosettes of different shapes and sizes were observed in the grainstone clasts (Figure 9a–f), distributed amongst the filamentous and unicellular microfossils described above. These are divided into four categories (types 1–4: Table 1). Type 1 star-shaped rosettes (Figure 9a) occur in close association with one another and average 20–25 µm in diameter. They typically consist of 7–15 filaments (≤1.5 µm wide by 10 µm long) arranged evenly around a central point, in an asterisk-like shape. Type 2 star-shaped rosettes are a similar size (averaging 25 µm in diameter) but comprise very wavy, sinuous filaments <1 µm wide by ≥10 µm long (Figure 9b,c). Type 3 star-shaped rosettes contain an opaque central core much larger than the length of the filaments, which are short (5–8 µm) and tapering (Figure 9d,e). Type 4 star-shaped rosettes also contain an opaque central core, but filaments extending from the core are longer (~15 µm), straight, and do not appear to taper (Figure 9f; Figure S3A). None of the star-shaped rosettes (types 1–4) display convincing examples of branching, however, these microfossils do bear similarities with *Eoastrion* Barghoorn from the c. 1.88 Ga Gunflint Iron Formation (Barghoorn & Tyler, 1965).

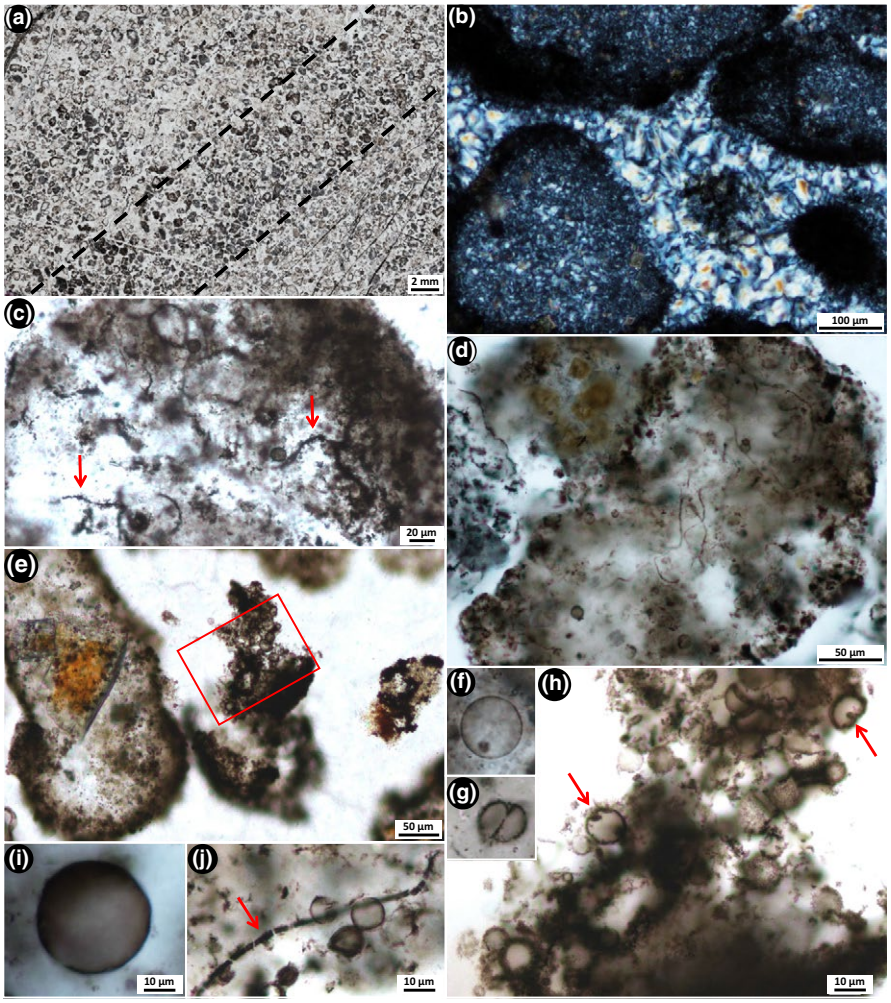

FIGURE 8 Bedded black chert texture and microfossils. (a) Bedded black chert consists of well-rounded, elongate to cuspate clasts of organic material and microfossils. Dashed lines highlight bedding. (b) Quartz crystals within clasts are much finer-grained than those outside of clasts, indicating two phases of silica precipitation. (c, d) Close-up of organic-rich clasts containing unicellular and filamentous microfossils. Some filaments have patchy, degraded outlines (arrows in c). (e) A clast densely packed with unicells. Red box shows location of (h). (f) Type 3 unicell (~19 µm diameter) with internal organic material. (g) Possible dividing unicell: two oval-shaped cells enclosed by an outer wall, with a straight shared inner wall (septum?). (h) Type 2 and type 3 unicells are quite closely associated with one another and are hollow with a continuous cell wall, not dense and grainy like those in the nodular black chert in Figure 4f. Note the internal organic masses within two of the type 3 unicells (arrows). (i) Very large unicell (type 4: ~35 µm in diameter). (j) Filamentous microfossil (type 6) with possible preserved cells (arrow), alongside unicellular microfossils. Scale for (f) and (g) is same as bar in (h) (10 µm) [Colour figure can be viewed at wileyonlinelibrary.com]

2.4.4 | Umbrella-like rosettes

Umbrella-like rosettes were observed within the grainstone clasts and are much less abundant than the star-shaped rosettes. Umbrella-like rosettes consist of a "mantle" ~37 µm by ~55 µm across, with vein-like filaments radiating out from a central point (Figure 9g). A thin membrane drapes over and between the filaments, resulting in a distinctive umbrella-like appearance. Associated with these microfossils are single filaments that appear to connect to, and extend away from, the central mantle (e.g., arrow in Figure 9g). There are also a number of unicells above and below these microfossils (i.e., not shown, but within the focal depth of the thin section) that may also be associated with these structures. However, the surrounding organic material is quite densely packed, resulting in an obscured view of the connecting components. These umbrella-like rosettes resemble *K. umbellata* described by Barghoorn and Tyler (1965) from the c. 1.88 Ga Gunflint Iron Formation.

2.4.5 | Branching filamentous rosettes

Large, complexly branching filamentous rosettes, 75–100 µm in diameter, were observed in between grainstone clasts (Figure 9h–j). These rosettes consist of relatively large, commonly gently curved filaments, ~3 µm wide and ~35–55 µm long, which are joined at a central point. Each of the main filaments branch three to four times (arrows in Figure 9h), into thinner, ~1–1.5 µm wide filaments, creating a dense and complicated framework-like structure. A web-like membrane connects most of the filaments (Figure 9i) and, in one example, a single unicell (~14 µm diameter) is observed in amongst the branching filaments (arrow, Figure 9i), but it is unclear if this is attached to—and thus part of—the branching microfossil structure, or a separate unicell entangled amongst the branches.

2.4.6 | Film coating grainstone clasts

Most of the kerogenous clasts in the grainstone are coated by a thin (~2 µm thick), typically highly convoluted, kerogenous film (Figure 10a,b; Figure S3D). These films also occur as detached sheets in between clasts (Figure 10c–e). The films are commonly highly ornate (Figure 10b), with a fine, granular, dimply texture and what appear to be cracked surfaces in places (arrows in Figure 10e). The films generally encircle the grainstone clasts, but are attached to the clasts only at spaced points, commonly appearing to float around and above the clasts.

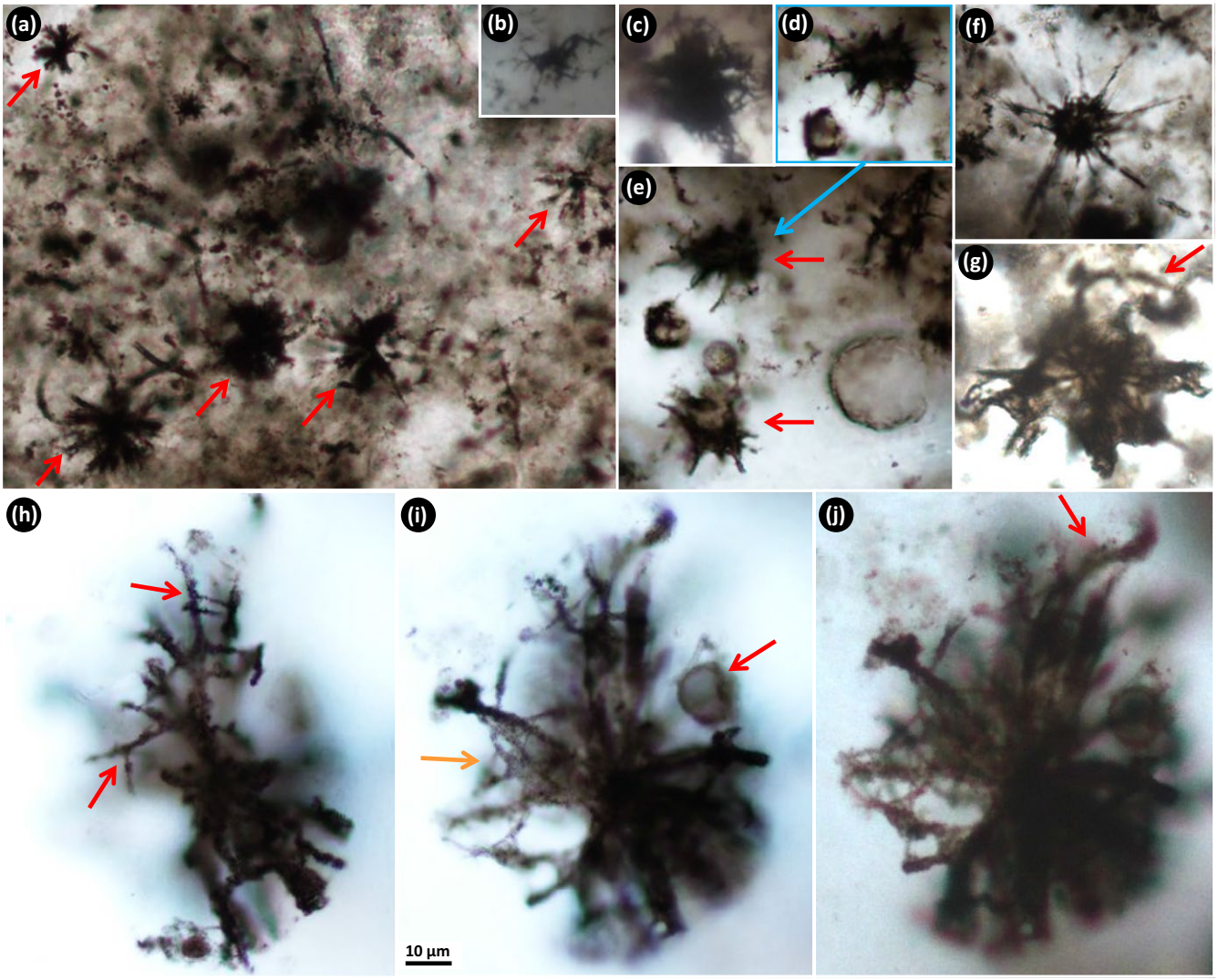

FIGURE 9 Microfossils in the bedded black chert, continued. Scale bar in i = 10 µm, for a–j. (a) Type 1 star-shaped rosettes with short, stubby filamentous structures arranged in an asterisk-like shape. Note the individual filamentous forms (type 6) also visible. (b, c) Type 2 star-shaped rosettes, with wavy, sinuous filamentous structures. (d, e) Type 3 star-shaped rosettes (red arrows), with large, opaque central cores and short, tapering filamentous structures. (d) is same specimen as in (e), at a different focal depth. Note the unicells (types 2 and 4) in (e). (f) Type 4 star-shaped rosette, with opaque central core and longer, straight filamentous structures. (g) Umbrella-like rosette consisting of radiating vein-like filamentous structures draped by a membrane. A curved filament, or possible stipe-like structure, is visible above the main fossil body—although slightly out of focus in this view (arrow). Single unicells are out of focus in the current view, but are present above, below and to the side of the main body. (h–j) A specimen of the large, complexly branching filamentous rosette at different focal depths. Note this microfossil morphotype is 3–4 times larger than the small, unbranching star-shaped rosettes in (a–f). (h) Arrows highlight multiple levels of branching along single filamentous structures. (i) A web-like membrane connects between filaments (orange arrow), and a unicell (red arrow) is present amongst the branches. It is not clear whether the unicell is part of the branching filamentous rosette structure, or an isolated cell trapped and preserved there. (j) The figure shows whole width of branching filamentous rosette microfossil: arrow highlights thicker, curved filament [Colour figure can be viewed at wileyonlinelibrary.com]

3 | DISCUSSION

3.1 | Biogenicity of kerogenous structures

All microfossil morphotypes described here from the TCG nodular and bedded black cherts are syngenetic to the chert samples and are composed of kerogen (Figures S1–S3). Most microfossils are a rich, medium to dark brown colour and are quite well preserved, reflecting the low temperature of metamorphism (~280 ± 30°C) estimated by Fadel et al. (2017). The biogenicity of key morphologies from the TCG is discussed below, specifically, the new forms presented (spherical aggregates and large, complexly branching filamentous rosettes), as well as microfossils that resemble forms reported previously from other correlative and younger sites, whose biogenicity has been questioned.

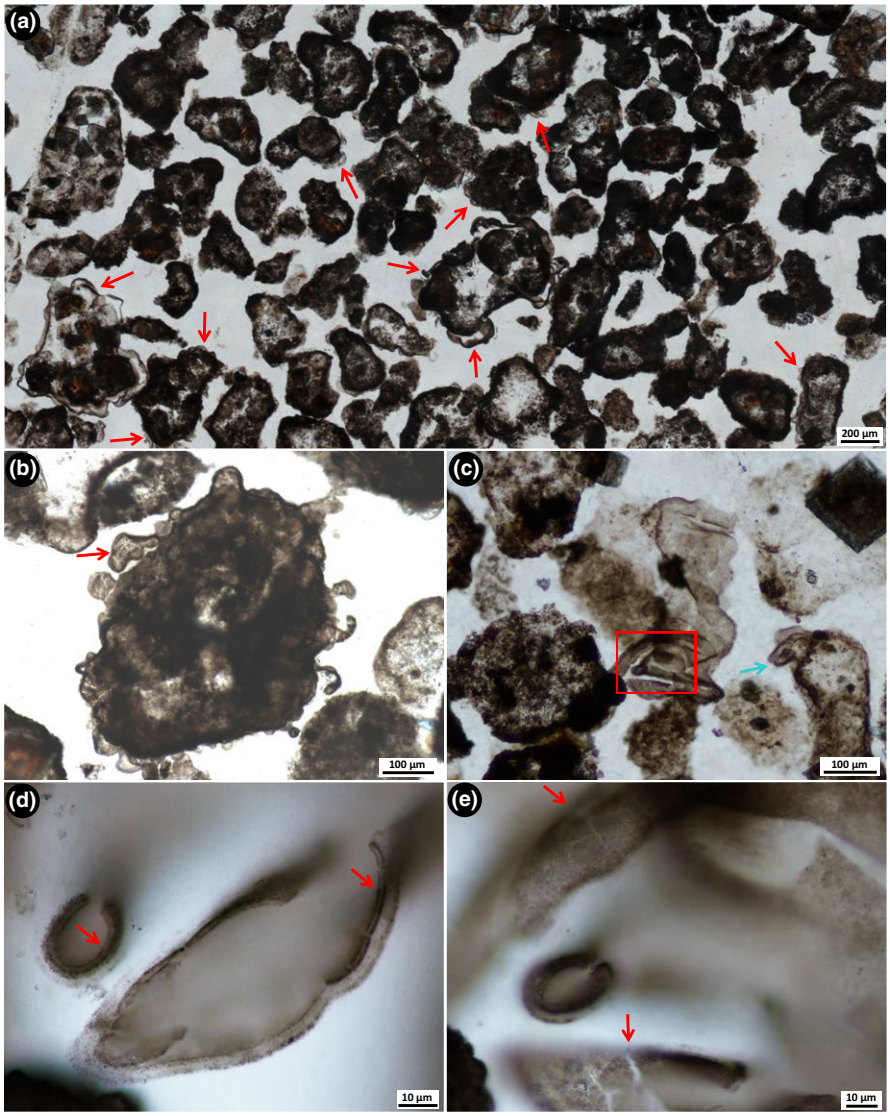

FIGURE 10 Kerogenous films within the bedded black chert are thin (~2 µm), have a granular, dimply texture and are cracked in places. (a) Large-scale stitched image of organic-rich grainstone clasts, with films encircling most clasts (e.g., arrows). (b) Close-up of an organic-rich clast with film coating, creating knobby, bent, hollow protrusions. Some surfaces of the knobs are cracked (faint white lines: e.g., arrow). (c) Films are occasionally observed as sheets between clasts. Red box shows location of (d, e), and blue arrow points to location of Raman spectroscopy map in Figure S3D. (d) Close-up of interclast film from (c). Note the film thickness of ~2 µm (arrows), with a granular and dispersed halo spreading away from the film, possibly due to the mobilisation of organic matter during quartz precipitation. (e) Same location as (d), but at a different focal depth. Note the granular, dimply texture and cracks (arrows) [Colour figure can be viewed at wileyonlinelibrary.com]

3.1.1 | Fine filamentous rosettes

The quality of preserved microfossils is related to diagenetic degradation and alteration; an increase in heat and pressure can cause changes to the texture and shape of a microfossil (Knoll et al., 1988). These changes can include condensation and granularisation; a colour change from dark brown to black; and mobilisation of organic matter along crystal boundaries (Knoll et al., 1988). For example, Knoll et al. (1988) observed piliform structures up to 7 µm in length and 0.5 µm in width along the outside of a larger filamentous microfossil. These piliform structures were attributed to the redistribution of organic material (see figure 12C in Knoll et al., 1988). This observation mirrors the quartz precipitation effects in an induced fossilisation experiment by Oehler (1976b), who demonstrated that redistributed organic matter along fibrous quartz crystal boundaries can produce fine, short (≤4 µm) and spiky filament-like shapes. In this experiment, organic matter was also mobilised ahead of the spherulitic quartz growth fronts to produce an irregular and patchy, almost sheath-like, rim of organic matter (see figure 5J in Oehler, 1976b).

This abiogenic form closely resembles the "globose colonies" of thin radiating filaments reported by Tyler and Barghoorn (1954) from the Gunflint Iron Formation. These thin, ~10–13 µm long filamentous forms radiate from a dense central core and are surrounded by an outer sheath, ~125 µm in diameter, which encompasses, but sits a considerable distance apart from, the radiating filaments (see figures 1 and 2 in Tyler & Barghoorn, 1954). Due to the similarity in morphology to the abiogenic forms produced by Oehler (1976b), and the location of the globose colonies in amongst spherulitic quartz, an abiogenic origin has been argued for these radiating filamentous structures (Awramik & Barghoorn, 1977; Oehler, 1976b).

The fine filamentous rosettes presented here from the TCG nodular cherts bear some similarity to those from Tyler and Barghoorn (1954), in that both examples are commonly found within fibrous quartz and consist of a mass of thin (~0.5 µm wide) filamentous structures that radiate out from a central point (Figure 6). Thus, it is conceivable that the TCG fine filamentous rosettes could have been produced by the migration of organic matter during fibrous quartz crystal growth (Oehler, 1976b). In this abiogenic hypothesis, the thin

filamentous forms could have originated as a clump of organic matter that quartz spherulites nucleated on, causing parts of the organic material in the clump to spread along and between the fibrous quartz crystals, creating fine radiating filaments morphologically similar to microfossils. On the other hand, in a case of the chicken and the egg: if there are rosette-splays of thin filamentous micro-organisms present before silicification, then radial, fibrous quartz may be precipitated in alignment with the filaments.

Several observations that may help clarify the origin of the TCG fine filamentous rosettes are outlined below:

1. Numerous examples of clots of organic matter directly beside the fine filamentous rosettes are not redistributed in elongated or filament-like shapes, despite also lying within fibrous quartz, and despite some clots being the nucleation site for silica spherulites (Figure 6a,b,d,e);
2. Some fine filamentous rosettes appear to be within quartz that is neither fibrous, nor spherulitic, but finely granular (see Figure 6e: rosette on right-hand side);
3. None of the fine filamentous rosettes observed in the Turee Creek nodular black cherts have a rim of surrounding organic matter like the "sheaths" in Tyler and Barghoorn (1954) or the rims in the induced abiogenic forms in Oehler (1976b);
4. The thin filamentous microstructures described here are much longer, 20–30 μm in length, compared to those in Tyler and Barghoorn (1954; ~10–13 μm in length) and to the abiotic versions in Oehler (1976b; ≤4 μm in length);
5. The thin filamentous microstructures are also commonly wavy along their length (see red arrows in Figure 6d), whereas abiogenic varieties in Tyler and Barghoorn (1954) and Oehler (1976b) mirror the largely straight growth of the fibrous silica crystals;
6. The Turee Creek fine filamentous rosettes show a range of occurrences, not just as isolated radiating splays, but also as clusters emanating out from the surface of larger filamentous microfossils, and from organic material (not shown in figures here); and,
7. The morphology of the fine filamentous rosettes described here is very uniform, with a high degree of repeatability in both the size of the rosettes, and of the individual filaments that comprise the rosettes. Such uniformity is unexpected should the forms arise through redistribution of organic matter, which ought to produce a variety of sizes depending on the degree of remobilisation and the rate of silica nucleation and crystallisation.

Combined, these observations lend weight to a primary, microfossil origin for the fine filamentous rosettes, however, a few of the points above could equally argue for a migration origin. Thus, further analysis is required to confirm the biogenicity of these organic microstructures.

3.1.2 | Spherical aggregates

An argument for the abiological origin of the cells that comprise the spherical aggregates could centre on the formation of these cells by the redistribution of originally dispersed organic matter around mesocrystalline quartz crystals. However, this is considered unlikely, as the very fine grain size of quartz that occurs within these microfossils is an order of magnitude finer than the cells themselves. Furthermore, the microquartz in the halo surrounding the spherical aggregates is also very fine-grained, yet there are no cellular structures within this outer halo (Figure 7). Thus, the cellular forms making up the aggregates cannot be the result of remobilisation around quartz crystals.

3.1.3 | Unicells with intra-cellular organic masses

Some of the unicells in the bedded black chert grainstone clasts contain distinctive, intra-cellular organic masses (Figure 8f,h), which could be the remains of a nucleus or other internal cellular structure (e.g., Oehler, 1976a). These organic masses also could have formed from degraded, collapsed and/or shrunken cells, with the remaining spherical outline being the preserved sheath or envelope (Golubic & Hofmann, 1976; Hofmann, 1976). Alternatively, the organic masses could have resulted from postmortem degradational effects (Hofmann, 1976; Knoll et al., 1978). At this stage, therefore, the likely origin of the organic masses inside some of the unicells in the bedded black chert grainstone clasts is unclear.

3.1.4 | Branching filamentous rosettes and star-shaped rosettes

Both the large, complexly branching filamentous rosettes from within the matrix of the Turee Creek bedded chert grainstone and the smaller, star-shaped *Eoastrion*-like rosettes found within the grainstone clasts resemble, at least in broad overall morphology, the modern form *Metallogenium*. *Metallogenium* is a ~2–15 μm wide rosette-shaped bacterium with flexible tapering filaments, on the end of which form spherical bodies, through which these bacteria are thought to multiply (Klaveness, 1977; Reitner, 2011; Zavarzin, 1981). *Metallogenium* could be a manganese and iron oxidiser, as it is often encrusted in these elements (Klaveness, 1977; Zavarzin, 1981), however, its biological affinity is still unknown (Klaveness, 1999; Reitner, 2011). Thus, the ancient equivalent, *Eoastrion*, could represent a fossilised metal-oxidising micro-organism (Knoll et al., 1988). Alternatively, as *Eoastrion* does not contain any convincing cellular parts (Klaveness, 1977), it is possible that it formed as the result of the radial displacement of organic matter during diagenesis; a recent nanoscale study could not find diagnostic evidence for, or against, a biogenic origin (Lekele Baghekema et al., 2017). However, the fact that *Metallogenium* and *Eoastrion* have been described from a range of living and fossil discoveries, including back to c. 2.4 Ga (this study), in each case with consistently similar features in terms of size and shape, and within assemblages of microfossils of undisputed origin (e.g., cellularly preserved filamentous microfossils and unicells showing cell division), strongly suggests that *Eoastrion* is a bona fide microfossil. Whether *Eoastrion* and *Metallogenium* represent the same micro-organism remains to be determined.

3.1.5 | Kerogenous films

An abiogenic method for the formation of the commonly ornate organic films coating the grainstone clasts could be that the films were formed from the remains of various organic components adsorbing or polymerising onto the clasts, or coating early diagenetic knobby cements. However, the fact that the films occur both surrounding clasts and as separate films floating in the matrix between the clasts (Figure 10), and are observed to curl up along edges (e.g., Figure 10c–e), precludes these abiotic methods of film formation. As the films have a primary thickness of ~2 μm (i.e., where there is dense kerogen), surrounded by a secondary granular, slightly blurred halo ~2–3 μm thick, it is likely that some of the organic matter was redistributed away from an original film surface during silicification (see arrows in Figure 10d). Therefore, we conclude that the kerogenous films are most likely preserved EPS that enclosed the kerogen- and fossil-rich clasts, and were formed through microbial activity before the clasts were cemented together by the mosaic microquartz matrix.

3.2 | Comparison with Gunflint Iron Formation microfossils

Some of the microfossils in kerogenous grainstone clasts from the TCG bedded black chert facies are morphologically similar to microfossils from the younger (c. 1.88 Ga), shallow-water Gunflint Iron Formation, first described by Barghoorn and Tyler (1965). For example, the unicellular microfossils described here resemble both *Huroniospora* Barghoorn and *L. golubicii*. The smaller unicellular forms in this study (type 2: Figure 8g,h,j) resemble *Huroniospora*, and are in the same size range as these younger counterparts (1–16 μm in diameter: Barghoorn & Tyler, 1965). Barghoorn and Tyler (1965) described three species in this genus, based on differences in wall thickness and texture; *Huroniospora microreticulata*, *Huroniospora macroreticulata* and *Huroniospora psilata*. However, Awramik (1976) noted that the distinctions between the three species may vary due to abiotic factors, such as mineral precipitation or cell degradation during diagenesis. This was confirmed by Wacey et al. (2012), who used FIB-TEM to show that wall reticulation in *Huroniospora* resulted from small-scale redistribution of organic matter during nanocrystal silica precipitation. Similarly, Lepot et al. (2017) found that at the nanoscale, variation in cell wall thickness was correlated with quartz crystal distribution and cell diameter, noting an apparent true difference between thin-walled and thick-walled *Huroniospora* varieties. Thus, when combined with cell diameter and nanoscale analysis, cell wall thickness may be a valid classification feature.

The slightly larger (up to ~19 μm diameter) type 3 unicellular microfossils described here (Figure 8f,h) contain internal cellular masses, comparable to Gunflint *L. golubicii* unicells identified by Knoll et al. (1978: plate 1; 5–31 μm in diameter). In addition to the type 2 and 3 unicellular forms, a population of even larger (type 4) unicellular microfossils are preserved, which range in size from >30 to 47 μm in diameter (Figure 8i). These large unicellular forms do not fit the size distribution of *Huroniospora* Barghoorn (1–16 μm) or *L. golubicii* (5–31 μm, avg. 13.5 μm) type populations described in Barghoorn and Tyler (1965) or Knoll et al. (1978). The larger, type 4 unicellular microfossils described here could be a continuation in the size distribution of *L. golubicii*, except for the fact that the type 4 unicells do not have the internal organic structures that are common in *L. golubicii*, and they are up to 16 μm larger than those reported in Knoll et al. (1978). Therefore, we contend that the population of type 4 unicellular forms in the Turee Creek Group bedded black chert represents a distinct, separate type of unicellular microfossil.

Barghoorn and Tyler (1965) also documented two species of the filamentous microfossil *Gunflintia* from the Gunflint Iron Formation shallow-water deposit, both of which are known to be up to 300 μm long: *Gunflintia minuta* (~1–2 μm wide) and *Gunflintia grandis* (~2.5–5 μm wide). The internal cells of *Gunflintia* vary between equidimensional and two to three times longer than wide, and are generally characterised by constrictions around the septae (see figure 4 of Barghoorn & Tyler, 1965; and figure 2D,G and figure S13A of Lepot et al., 2017). The filamentous microfossils in the Turee Creek Group bedded chert grainstone clasts described here (Figure 8c,j; Figure S2C) could be comparable to *Gunflintia* Barghoorn, as they are a similar size (~1–2.5 μm wide and ~50–100 μm long) and have what appears to be a probable internal cell length of 4–9 μm. However, it is unclear whether the Turee Creek filamentous forms display the typical constrictions around the septae: some examples are too patchy and degraded to clearly see the internal cellular arrangement (Figure 8c; Figure S2C), and other examples with apparent cells (Figure 8j) lack evidence of the filament edges constricting around the septae. Thus, the Turee Creek filamentous microfossils from the bedded black chert facies could represent a different filamentous form altogether, as the outline of the filamentous microfossil in Figure 8j appears much smoother than the Gunflint filaments, with probable cells that are two to almost four times longer than wide.

Alternatively, the smoother Turee Creek filamentous forms could be *G. minuta* subtype 1 (Lepot et al., 2017), which are *G. minuta* morphotypes that consist of an organic tubular sheath, inside of which no cells or internal organic material are preserved. In this case, the cell-like segments in the Turee Creek filamentous microfossils could be the result of fragmentation of the micro-organism before, during or after silicification. However, we consider fragmentation before silicification unlikely, as the segments are at regular intervals. In a similar way, we consider fragmentation during or after silicification unlikely, as the immediately adjacent *Huroniospora*-like unicellular forms are unaffected by breakages in their structure. Overall, the type 6 filamentous microfossils presented here are too small and degraded to clearly determine whether they constrict at the septae, so we cannot definitively assign them to *Gunflintia*.

The star-shaped rosettes reported here (types 1–4: Figure 9a–f; Figure S3A) resemble *Eoastrion* Barghoorn from the Gunflint Iron Formation in both size and descriptive morphology. *Eoastrion* consists of a variable number of filaments, commonly sinuous, that radiate irregularly from a generally opaque central body, which varies in size (Barghoorn & Tyler, 1965). Two species of *Eoastrion* were

described by Barghoorn and Tyler (1965): *Eoastrion simplex*, with simple, radiating filaments; and *Eoastrion bifurcatum*, with bifurcating filaments radiating from a larger central core. Gunflint *Eoastrion* rosettes are ~10–30 μm in diameter with individual filaments ~1.5 μm wide and 3–18 μm long (Barghoorn & Tyler, 1965; Cloud, 1965).

Although it is not clear whether individual filaments bifurcate in the Turee Creek examples, or just overlap other filaments within the focal depth of the slide, the similarities in size and morphology between the TCG star-shaped rosette microfossils and *Eoastrion* Barghoorn from the Gunflint Iron Formation are striking. We report four different types of star-shaped rosettes from the Turee Creek assemblage (types 1–4; Figure 9a–f). The overall size ranges (~20–35 μm) and filament dimensions (≤1.5 μm wide by 5–15 μm long) of these four types are comparable to Gunflint *Eoastrion* rosettes. Type 1 star-shaped rosettes of the Turee Creek Group assemblage are ~20–25 μm in diameter (Figure 9a) and resemble both *E. simplex* from Barghoorn and Tyler (1965: see figure 6, parts 2–6) and *Eoastrion* "type 1" from Lekele Baghekema et al. (2017: see figure 4E, ~13 μm diameter). However, it should be noted that Turee Creek type 1 rosettes also look similar to *K. umbellata* Barghoorn, without the spheroidal bulb (e.g., figure 7, part 10 of Barghoorn & Tyler, 1965). In a similar way, Turee Creek type 2 star-shaped rosettes (Figure 9b,c) closely resemble *E. bifurcatum* (see figure 6, part 7 of Barghoorn & Tyler, 1965), albeit the Turee Creek examples have a more tangled nature. Turee Creek type 3 star-shaped rosettes (Figure 9d,e), which contain a large opaque central core and short, tapering filaments, resemble yet other described examples of *E. bifurcatum* (see figure 5, part 2 of Barghoorn & Tyler, 1965). Turee Creek type 4 star-shaped rosettes, which are up to ~35 μm across and consist of a central core and long, straight filaments, do not directly resemble *Eoastrion* forms described by Barghoorn and Tyler (1965). However, they do appear similar to "type 2" *Eoastrion* identified by Lekele Baghekema et al. (2017), although these younger forms are much smaller (~22 μm diameter) than those described here.

The umbrella-like rosettes from the Turee Creek bedded black chert clasts (Figure 9g; Figure S3B) distinctly resemble *K. umbellata* from the Gunflint Iron Formation (Barghoorn & Tyler, 1965). *Kakabekia umbellata* specimens consist of a tripartite structure: a crown or mantle (5–30 μm in diameter), a stipe, and a bulb (Barghoorn & Tyler, 1965). The crown contains radiating, vein-like thickenings that extend from a central point and are covered by a membrane, creating the umbrella-like shape. The TCG umbrella-like rosettes are similar, in that these also contain a mantle with a thin membrane that connects radiating, vein-like filaments, as well as a stipe and nearby unicells that are comparable to possible bulb-like structures (Figure 9g; Figure S3B), although the connections between the stipe and bulb parts of the Turee Creek example are obscured by the relatively densely packed surrounding organic material.

Gunflint-type microbiota are found in multiple other localities worldwide, ranging from c. 1.6 Ga through to c. 2.1 Ga, including the c. 1.6 Ga Barney Creek Formation (Oehler, 1977), c. 1.65 Ga Paradise Creek Formation (Cloud, 1976), c. 1.8 Ga Duck Creek Dolomite (Knoll & Barghoorn, 1976) and c. 1.88 Ga Frere Formation (Tobin, 1990) in Australia; the c. 1.88 Ga Sokoman Iron Formation in Canada (Knoll & Simonson, 1981); the c. 2 Ga Tyler Formation in Michigan, USA (Cloud & Morrison, 1980); and the c. 2.1 Ga Franceville Group in Gabon (Amard & Bertrand-Sarfati, 1997; Lekele Baghekema et al., 2017). It has been noted previously that the presence of Gunflint-type microfossils across a wide age range (~500 Ma) is best explained by microbiota representative of a particular Paleoproterozoic environment, rather than a specific biostratigraphic horizon (Hofmann, 1976; Knoll & Simonson, 1981; Lepot et al., 2017; Tobin, 1990). That is, the Gunflint microfossils are generally preserved by early silicification in stromatolitic units from subtidal settings (Awramik & Barghoorn, 1977; Lanier, 1989). The oldest currently known examples of Gunflint-type microbiota are from the c. 2.1 Ga Franceville Group in Gabon (Amard & Bertrand-Sarfati, 1997; Lekele Baghekema et al., 2017). Thus, the presence of Gunflint-type microfossils in the TCG microfossil assemblage highlights the persistence of silica-rich subtidal microbial environments throughout the Paleoproterozoic (Tobin, 1990), and pushes the occurrence of Gunflint-type microbiota back a further ~300 Ma, to c. 2.4 Ga.

3.3 | Two distinct microfossil communities

Two distinct communities of microfossils have been discovered within separate nodular and bedded facies of black chert within the Turee Creek Group outcrops studied here.

1. Nodular cherts, from within the interbedded shale and ironstone sequence, contain three clear groups of textures that originate from separate samples of nodular chert within the same sequence. Texture 1 consists of a variety of microfossils tangled in a web-like network that wraps around ellipsoidal to partly polygonal domains of coarse mosaic to spherulitic microquartz. Separate samples of nodular chert from the same sequence contain the narrow, straw-like filaments encircling clusters of framboidal pyrite (texture 2), and still other samples preserve the spherical aggregates within layers of dense clumps of elongated organic matter and abundant, small organic clots (texture 3). In summary, microfossil types present within nodules include filamentous microfossils (types 1–4); dense, type 1 unicells of one size distribution (~20 μm); straw-like (type 5) filaments up to 575 μm in length; fine filamentous rosettes with extremely thin (0.4 μm), short filamentous microstructures; and a distinctive type of microfossil consisting of relatively large (up to 138 μm in diameter), spherical aggregates of cells.
2. Microfossils observed in the bedded black chert facies are entirely distinct from those of the nodular chert, with no overlapping "species" between the two. The microfossils are preserved mostly *within* rounded to cuspate clasts of organic material (9 morphotypes), but one morphotype is found within the matrix material between the clasts. The microfossil assemblage within the clasts consists of: three categories of unicells based on size (types 2–4); filaments that are often degraded (type 6:

~50–100 μm long); star-shaped rosettes (types 1–4: ~25 μm wide); and umbrella-like rosettes, ~37–55 μm wide. Large, complexly branching filamentous microfossils (75–100 μm in diameter) are preserved *in between* the kerogenous clasts.

3.3.1 | New microfossil occurrences

Two new microfossil morphologies are reported here: spherical aggregates from nodular black chert samples and large, complexly branching filamentous rosettes from bedded black chert samples.

The spherical aggregate microfossils are relatively large, up to 138 μm in diameter, and have a distinct, honeycomb-like appearance due to the aggregated nature of the comprising cells (Figure 7). These microfossils are permineralised within very fine-grained microquartz that extends out into a perfectly spherical rind that evenly surrounds each aggregate. This outer rind, or halo, is clear of the clots of kerogen that fill the space beyond the aggregates (Figure 7d; Figure S1E), which may suggest an outer envelope (which could be the remains of a capsule or EPS?) associated with this microfossil. Thin, often bent, kerogenous structures project from the main body of the aggregates out into the halo (e.g., Figure 7; Figure S1E). These irregular structures could be explained in a number of ways: a primary feature of the structure of the microfossil, such as flagella, which would help it to move; the edges of cells that ruptured to release spores or were unintentionally burst due to environmental pressure; or degradation of the structure after cell death but before preservation, giving the impression of processes. The spherical aggregate microfossils, with their large size, consistent spherical structure and unique kerogen-free halo, are unlike any other forms known from either older or younger rocks, and thus, are considered here a new microfossil form.

The large, complexly branching filamentous microfossils (Figure 9h–j) are broadly similar in overall shape to other rosette forms, such as *Eoastrion* and *Kakabekia* from the Gunflint Iron Formation, as well as the star-shaped rosettes (types 1–4) and the umbrella-like rosettes described here. However, we consider this larger, complexly branching filamentous microfossil to be a distinct morphospecies, based on its significantly larger size (three to four times larger than *Eoastrion* rosettes, and two to three times larger than *Kakabekia*, based on average radii) and the complex nature of the branching. In particular, the large structures described here contain clear examples of multiple levels of filament branching, away from a central node, which creates an intricate framework-like structure (Figure 9h) that supports a fine, membranous web-like fabric (Figure 9i). This complex framework structure is quite distinct from anything previously described from the Gunflint, or any other unit (Amard & Bertrand-Sarfati, 1997; Awramik & Barghoorn, 1977; Barghoorn & Tyler, 1965; Cloud, 1976; Knoll & Barghoorn, 1976; Knoll et al., 1988; Schopf et al., 2015; Wilson et al., 2010), and we therefore propose that this microfossil should be classified as a distinct, new form.

3.3.2 | Preservation of Turee Creek Group microfossil communities

Studies show that microbial decomposition occurs in the order of days to weeks (Bartley, 1996; Decho, Visscher, & Reid, 2005), so that in order to become fossilised, any microbial life must be buried or permineralised relatively quickly. The vast majority of Precambrian microfossils are preserved in cherts, or stromatolites that were silicified early (e.g., c. 3.4 Ga Strelley Pool Fm: Sugitani et al., 2010; c. 3.3 Ga Buck Reef Chert: Walsh & Lowe, 1985; c. 3 Ga Farrel Quartzite: Sugitani et al., 2007; c. 2.5 Ga Gamohaan Fm: Czaja et al., 2016; amongst others). Less commonly, microfossils are preserved in shales (e.g., c. 1.5 Ga Roper Group: Peat, Muir, Plumb, McKirdy, & Norvick, 1978; ≥1.4 Ga Ruyang Group: Yin, 1997), but rarely are microfossils preserved in carbonates due to the destructive nature of carbonate crystal growth (Grotzinger & Knoll, 1999; Schopf, Kudryavtsev, Czaja, & Tripathi, 2007). Thus, early permineralisation by silica plays a critical role in preserving the morphology of micro-organisms.

The two communities of TCG microfossils presented here are predominantly very well preserved and the microfossil morphologies are demonstrably primary; their arrangement appears to be unaffected by silica growth (e.g., Figures 4c,d and 5c,d). Evidence at outcrop and thin section scale of both the nodular and bedded black chert units indicates very early silicification of the microfossils. For example, outcrop observations of the interbedded shale, ironstone and dolosiltite layers bending around the black chert nodules (Figure 2c,d) highlights silicification of the nodules prior to compaction arising from sediment burial. This is reflected in thin section, where the spherical nature of both the unicellular and spherical aggregate microfossils points to silicification before even slight burial or compaction by overlying sediments. In addition, there are multiple examples of very well-preserved microfossils and associated morphological features, including the filamentous microfossil life array (Figure 4e), the tangled filamentous network (Figure 3), the probable cellular compartments within filaments (Figure 4b), the preservation of very thin filamentous microstructures (~0.4 μm wide) in the fine filamentous rosettes (Figure 6), and the cells of the spherical aggregate microfossils (Figure 7). Spectacularly, the web-like membranous material draping the large branching filamentous rosette microfossils from the bedded black chert (Figure 9i), and the delicate, highly ornate external structures of the microbial EPS coating of some of the grainstone clasts (Figure 10a,b), also point to very early silicification.

Evidence for two generations of early silica precipitation is present in the bedded black chert. Thin section observations show fine, granular microquartz within the grainstone clasts, whilst silica radiates from the outside of clasts and fills the interclast space with a medium-grained mosaic of microquartz (Figure 8b). This indicates that the first generation of silicification (and likely mineralisation of some of the organic carbon to carbonate) occurred within the clasts and a second generation of silica cemented the clasts together. The first generation of silicification likely initiated in shallower water, or possibly in the water column (Siever, 1992),

supported by the rounded (not flattened) nature of the grainstone clasts and the preservation of perfectly spherical unicells inside the organic-rich clasts. The second generation of silicification, cementing the clasts together, would have had to occur rapidly to preserve the organic content (Figure S3D) of the films interpreted as EPS, as a study on the decomposition of EPS shows ~30%–50% loss of C (as $^{14}CO_2$) in 48 hr (Decho et al., 2005). That this second generation of interclast silicification was also early is further supported by the grainstone clasts being uncompacted and touching only on points (Figures 8a and 10a; Lanier, 1989). In summary, to preserve microfossils both within the transported clasts (unicells, filaments, star-shaped *Eoastrion*-like rosettes and *Kakabekia*-like rosettes) and between the transported clasts (large branching filamentous rosettes, as well as the EPS films), two generations of silicification must have occurred rapidly, before compaction of the grainstone and diagenesis.

The composition of the Proterozoic ocean is thought to have been high in dissolved silica (Maliva, Knoll, & Simonson, 2005; Siever, 1957; Xiao, Schiffbauer, McFadden, & Hunter, 2010). Silica precipitation would likely have initiated both in the water column and at the sediment-water interface, as a result of a sequence of chemical reactions involving microbial degradation, pH changes, and silica diffusion gradients between the sea water and buried sediments (Siever, 1992). The relationship between these factors is complex, but accounts for the multiple phases of early silica precipitation apparent in both the nodular and bedded black cherts described here.

3.4 | Reconstructed basin model

Compiled stratigraphic sections by Barlow et al. (2016), along with new field observations from this study, highlight the relationships between different facies at this locality. A shallow-water stromatolite-thrombolite reef complex at the base of the succession passes up through turbiditic dolarenites, to thinly bedded dolosiltites interbedded with bedded black chert units. This is followed by deposition of ironstone with black chert nodules that transitions up-section into shale. This succession partly repeats itself in reverse up stratigraphic section, passing from shale to interbedded shale and ironstone with black chert nodules, grading to ironstone with chert nodules, followed by layers of finely bedded dolosiltite interbedded with bedded black chert units. The dolosiltites are interpreted to represent the far distal toes of the coarser-grained, underlying carbonate turbidites. Very fine layering in dolosiltite beds and ironstone and shale units, along with a lack of sedimentary structures characteristic of storm currents (e.g., hummocky cross-stratification), indicates that these deeper-water units—including the bedded and nodular black cherts studied here—were deposited below storm wave base (~50–250 m: Flugel, 2004), and thus could also have been deposited below the photic zone. The ironstone–nodular black chert sequence is interpreted to represent a likely ferruginous chemocline within the Paleoproterozoic ocean because of the abundant siderite, haematite and manganese oxide present in these rocks (Figure 2c; Barlow et al., 2016).

These facies relationships were used to reconstruct a representative depositional basin model (Figure 11) using Walther's Law, which states that superimposed strata reflect different parts of the basin juxtaposed through transgression/regression events. In this reconstructed basin model, the relative position of the shallow-water microbialites are based on data from Barlow et al. (2016), whilst the relative position of the deeper-water units are based on stratigraphic transects from this study (see summary in Figure 2a, right-hand side). The shale has been positioned as the deepest-water unit in the succession, as it was interpreted to have been deposited at the point of a basin inflexion during the transition between transgression and regression events (Barlow et al., 2016).

The nodular and bedded black cherts are deposited in similarly deep-water sections of the stratigraphy, yet they preserve distinct, separate communities of microfossils from different environments: a deeper-water, primarily benthic *in situ* community in the nodular cherts, and, a primarily transported, originally shallower-water community that is now preserved in the deeper-water bedded black cherts (described below).

3.4.1 | Nodular black chert

The microfossils preserved in the deep-water nodular black cherts described here from the TCG dolomite ridge locality are interpreted as a primarily benthic assemblage. The tangled network of filamentous and unicellular microfossils in texture 1 likely grew in the sediment and/or on the seafloor. The ellipsoidal clear domains in the tangled filamentous network contain multiple stages of silica growth. The outermost parts of these clear domains are characterised by a rim of microcrystalline quartz that appears to nucleate from the edges of the tangled networks (Figure 3d). The quartz coarsens inwards to a macrocrystalline quartz mosaic, with the core of the clear domains occasionally chalcedonic (Figure 3c,d). This multi-stage growth could have filled primary void spaces, or replaced a pre-existing material (e.g., anhydrite—see: Chowns & Elkins, 1974; Milliken, 1979). Either way, it shows that the tangled distribution of this filamentous-unicellular microfossil network is likely a primary feature, indicating a seafloor or subseafloor habitat for these microfossils, as previously suggested by both Schopf et al. (2015) and Fadel et al. (2017) for similar occurrences.

In addition, the presence of the alternating vertical-horizontal filamentous microfossils described here (also part of texture 1: Figure 4e; Figure S4) provides direct evidence for the tangled network being an *in situ* assemblage. These alternating filaments are clearly a life array with permineralised micro-organisms that were likely preserved in a matter of days. Such an arrangement is typical of phototrophic microbial communities in modern shallow-water stromatolites and hot spring sinters, and has been explained by both daily and seasonal cycles: day or summer results in a vertical orientation, and night or winter a horizontal orientation (Berelson et al., 2011; Dupraz, Fowler, Tobias, & Visscher, 2013; Lanier, 1989; Mata et al., 2012; Monty, 1976; Ramsing, Ferris, & Ward, 2000; Ruff & Farmer, 2016; Turner, James, & Narbonne, 2000; Wagstaff

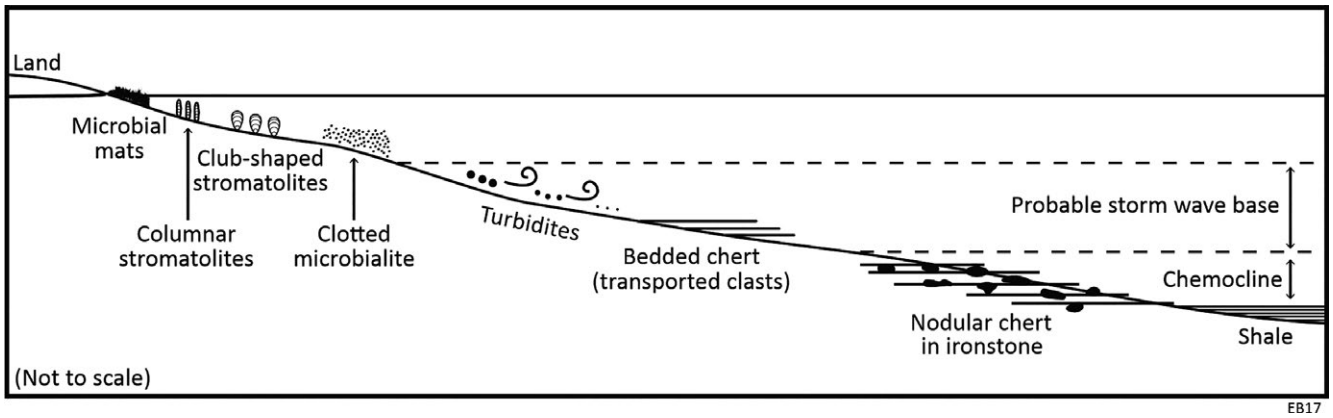

FIGURE 11 Model of the depositional basin showing the relationship between key units preserved in the Turee Creek Group dolostone ridge. The shallow-water stromatolite–thrombolite reef, described in detail by Barlow et al. (2016), passes through turbidites to the deeper-water units. The relative location of the bedded and nodular black chert units is shown, along with an indication of the probable storm wave base and relative depth of the interpreted chemocline. The shale represents the deepest-water unit in the preserved succession

& Corsetti, 2010; Walter, 1976). However, the filamentous forms in the life array described here are preserved in a deeper-water setting. Therefore, the alternating filament orientation could be explained by anoxygenic photosynthesis. Alternatively, if this life array assemblage lived below the photic zone, the vertical-horizontal orientation could be attributed to chemotrophy. For example, modern benthic filamentous sulfur bacteria in deep marine ecosystems are known to glide vertically between the sediment surface and subsurface, and sometimes abandon their sheaths to glide horizontally on the sediment surface (Schulz & Jorgensen, 2001; Schulz, Jorgensen, Fossing, & Ramsing, 1996). Other modern benthic long filamentous bacteria do not appear to glide, but instead, their long form bridges the gap between the sediment surface and deeper layers. These so-called cable bacteria transport electrons along their length between the two half-reactions of oxygen reduction at the sediment surface and sulfide oxidation in the subsurface (Nielsen, Risgaard-Petersen, Fossing, Christensen, & Sayama, 2010; Pfeffer et al., 2012). Thus, the vertical-horizontal arrangement of TCG filamentous forms could be the result of either phototrophic (likely anoxygenic photosynthesisers) or chemotrophic micro-organisms. Regardless of metabolic origin, this interesting arrangement shows that these filamentous microfossils were not transported and are preserved *in situ*, in life position.

In a similar way, the straw-like filamentous microfossils in nodular black chert texture 2 (Figure 5) are interpreted as a benthic assemblage, due to their exceptionally long length (up to 575 μm) that suggests little or no transport of these filamentous forms.

Despite also being preserved in nodular black cherts from the interbedded shale and ironstone sequence, spherical aggregate microfossils are not present in samples that contain the tangled (texture 1) or straw-like (texture 2) filamentous microfossils. Instead, spherical aggregate microfossils are observed within samples that have a distinctly different texture in thin section (texture 3), which consists of well-defined beds that contain dense clumps of organic matter elongated along bedding planes, along with abundant, small organic clots. The spherical aggregate microfossils are permineralised in very fine-grained microquartz, whilst the surrounding material is preserved in a coarser-grained quartz. This implies at least two phases of silicification and shows that the aggregates were preserved earlier than the surrounding material. Spherical aggregate microfossils within the well-defined bedding could have been either transported from elsewhere and deposited, or, benthic micro-organisms that lived on or in the organic-rich layers.

If the latter were the case and the spherical aggregate microfossils lived on the seafloor, or within the sediment, then the varying grain sizes related to the two phases of silicification could possibly be explained by preferential silicification of organic material. For example, microbial structures can be coated in a thin silica crust before later precipitation of the surrounding matrix (Konhauser, Phoenix, Bottrell, Adams, & Head, 2001). However, in a benthic interpretation, it is difficult to envisage a way in which the spherical nature of both the aggregates and the evenly spaced surrounding halo are preserved. On the seafloor (or in the sediment) the spherical aggregates would have been partly (or completely) surrounded by material, which would probably have resulted in an oval-shaped or elongated form, and an unevenly spaced, slightly flattened halo; neither of which are features observed here. That the spherical aggregates aren't affected by compaction, despite being preserved within layers that contain dense clumps of organic matter that are elongated along the bedding plane, makes a benthic interpretation less likely.

On the other hand, the spherical aggregates could have lived in suspension in the water column and dropped down into the deeper-water setting when they died. If this were the case, there would be little to influence the overall shape of the aggregates of cells except the naturally preferred physical state of tending towards a minimum surface area (i.e., a sphere). In this case, an even distribution of silica could start to form around the aggregates whilst still suspended, consistently preserving the spherical shape of both the aggregate and the surrounding halo (which could be remains of a capsule or EPS?). This process also explains the two phases of silicification present

in texture 3: the distinctly finer grain size within and immediately surrounding the aggregate microfossils, compared to the coarser quartz grain size present in the rest of the sample. Thus, owing to the consistent spherical nature of the aggregate microfossils and the distinctive, very fine-grained, evenly spaced and kerogen-free halo, we interpret these relatively large forms as in-fallen, possibly planktonic organisms, which could have dropped into the deeper-water units from above.

Metabolic interpretations

Both Schopf et al. (2015) and Fadel et al. (2017) described similar cobweb-like masses of tangled filamentous microfossils but proposed different interpretations of the likely metabolism of these micro-organisms. Schopf et al. (2015) interpreted this distinct assemblage, sampled from a Turee Creek Group locality ~65 km to the south-east of the c. 1.88 Ga Duck Creek Dolomite (lat. 22.48°S, long. 116.52°E), as a sulfuretum. This was based on morphological comparison with modern sulfur-cycling organisms, and S isotope data of pyrite from samples of a similar filamentous assemblage in black chert from the younger Duck Creek Dolomite (with $\delta^{34}S$ values ranging from −9.4 to +43.4‰); no pyrite was reported from within the Turee Creek Group cobweb-like assemblage.

Three of the filamentous microfossils from the tangled network reported here in the deep-water nodular black cherts from the TCG dolomite ridge locality resemble, in size and morphology, those discussed in Schopf et al. (2015) (Table 2). These include the 5–9 μm wide, type 2 filaments with dark and light banding (Figure 4b); the

TABLE 2 Comparison of filamentous microfossils reported here with others thus far described from the Turee Creek Group, by Schopf et al. (2015) and Fadel et al. (2017)

	This study		Schopf et al. (2015)	Fadel et al. (2017)
Location	Black chert sampled between 22°26.291′S, 116°27.888′E and 22°31.021′S, 116°33.151′E		~65 km to the south-east (lat. 22.48°S, long. 116.52°E) of the c. 1.8 Ga Duck Creek Dolomite	One microfossiliferous black chert sample from 22°29.748′S, 116°31.817′E
Filamentous microfossil types reported	Type 1	10–14 μm wide, >250 μm long	X	Possibly comparable to Fadel et al. (2017) "type 3" filaments: broad (3–10 μm diameter) with thin (30–100 nm) sheaths
	Type 2	5–9 μm wide and ~700 μm long, with ~12 μm long alternating dark (carbonaceous-rich) and light (carbonaceous-poor) bands	~7–9 μm diameter; possible elongated cells ~12–15 μm long	Probably comparable to Fadel et al. (2017) "type 2" filaments: thin central tubes bound by thick granular sheaths (total width 5–7.5 μm), with dark and light "striations" (possible cells)
	Type 3	1.4–3 μm wide, ~200 μm long	1–4 μm wide; possible bead-shaped cells	X
	Type 4	0.5–1.2 μm wide, 100's μm long	Narrow thread-like filaments, <1 μm wide	Not shown, but reports long thread-like filaments ≤1 μm diameter
	Type 5	3–4 μm wide, up to 575 μm long; smooth sheaths, no visible cells	X	Probably comparable to Fadel et al. (2017) "type 1" filaments: 2–3 μm wide with thin, continuous sheaths
	Type 6	1–2.5 μm wide, 50–100 μm long; with 4–9 μm long segments, possibly elongated cells	X	X
	X		X	Fadel et al. (2017) "type 4" filaments are categorised as such because they could not be distinguished from types 1–3. "Type 4" filaments are siderite-rich and highly degraded, with poorly preserved kerogen

Note. X: not present or not described in study. All other microfossil types documented in this study (see Table 1 for summary) are not detailed in Schopf et al. (2015) or Fadel et al. (2017).

1.4–3 μm wide type 3 filaments (Figure S1A,B; although, these are not obviously bead-celled like those described by Schopf et al., 2015); and the thin, 0.5–1.2 μm wide thread-like filaments (type 4: Figure 4c,d). The 3–4 μm wide straw-like (type 5) filamentous microfossils here (Figure 5a) are distinct from any of the filaments presented in Schopf et al. (2015), although they are probably comparable to "type 1" filaments of Fadel et al. (2017). The presence of fine-grained, framboidal pyrite associated with these long straw-like (type 5) filamentous microfossils may support a sulfuretum interpretation, although, a causal relationship between these filaments and pyrite crystals is yet to be demonstrated. All other microfossils within the nodular black chert are distinct from any forms described by either of the above authors, including; the larger 10–14 μm wide filaments (Figure 4a), the unicells (Figure 4f), the fine filamentous rosettes (Figure 6), and the spherical aggregates (Figure 7).

Fadel et al. (2017) also reported cobweb-like masses of filamentous microfossils from the Turee Creek Group, but from the dolomite ridge locality at 22°29.748′S, 116°31.817′E (see Figure 1). Described were three main types of filamentous microfossils, with a fourth category for those examples too poorly preserved to place in types 1–3 (see Table 2 for comparison with filamentous types documented here). The filamentous forms in Fadel et al. (2017) were variably replaced by siderite, which increased with decreasing preservation of microfossils. The siderite was suggested to derive from the reduction of Fe(III)-oxides, with filament types 2–4 interpreted as remains of iron-oxidising bacteria. Fadel et al. (2017) noted that the siderite is a later mineralisation feature, but suggested that the distribution of the cobweb-like networks is likely a primary feature of the microfossil community. Our observations support the distribution of the tangled networks as a primary feature, but none of the filamentous forms described here are visibly replaced by siderite under the petrographic microscope. Likewise, Schopf et al. (2015) noted a lack of siderite and did not report siderite replacement of any microfossils, although, nanoscale techniques were not used.

To account for the differences in interpretation of sulfur- vs. iron-cycling, and the presence vs. absence of iron-bearing minerals, Fadel et al. (2017) proposed that the filamentous forms preserved in the cobweb-like masses may have been able to cycle both sulfur and iron, as is the case with some modern micro-organisms. Additional work is currently underway, including carbon isotopic and nanoscale elemental analyses of the microfossils, and sulfur isotopic analysis of the pyrite, to try and account for the variability in the presence of iron associated with the cobweb-like fabric reported in Schopf et al. (2015) and Fadel et al. (2017). These analyses will provide additional insights into the probable metabolisms of the tangled filamentous forms, as well as the other microfossils from the TCG presented here.

3.4.2 | Bedded black chert

The rounded nature of the grainstone clasts, and the similarity of contained microfossils to the shallow-water Gunflint-type microbiota, suggests that the clasts were transported from shallower-water into the deeper-water setting in which they are preserved. We posit two ways in which this process may have occurred. In the first, the grainstone clasts could represent ripped-up pieces of microbial mat that once grew in the shallow waters of the intertidal zone of this succession and were rounded as they were washed down into the deeper-water setting, after a storm or other high-energy event. This is supported by evidence from the modern-day stromatolites at Shark Bay in Western Australia, which shows that rounded, centimetre-sized pieces of microbial mat form as a result of storm events (Figure 12a). This process is reflected in the shallow-water part of the Turee Creek stromatolite-thrombolite reef complex studied here, which contains thin conglomerate beds with subrounded clasts of ripped-up microbial mat preserved between stromatolite layers (Figure 12b). Clasts of ripped-up mat can be backwashed and transported through the stromatolite intertidal zone, become finer-grained the further they are transported away from the shore, and eventually be deposited as submillimetre-scale clasts in deeper water. The rounded nature of the bedded black chert grainstone clasts, as well as the sparse distribution and random orientation of the filamentous microfossils within the clasts, supports transportation (Tobin, 1990). Furthermore, the generally degraded nature of the filamentous microfossils in the grainstone clasts compared to those from the benthic community in the nodular black chert suggests a longer period of degradation, consistent with transport away from their source.

Alternatively, the grainstone clasts could have formed from floating, globular colonies of micro-organisms on, or near, the surface of the ocean, such as; flocs (Flemming & Wingender, 2001, 2010), suspended aggregates (Decho & Gutierrez, 2017), jelly bombs (Dupraz et al., 2013; Fowler, 2011; Helm & Potts, 2012), algal lumps (Monty, 1967; Walsh & Lowe, 1999), or organic aggregates (Riley, 1963, 1970; Riley, Van Hemart, & Wangersky, 1965; Riley, Wanngersky, & Van Hemart, 1964). Colonies of floating micro-organisms establish films of EPS designed to protect and keep the microbial community together (e.g., Decho & Gutierrez,

FIGURE 12 (a) Rounded clasts of microbial mat on the shore of Shark Bay, Western Australia, washed up after a storm event. (b) Subrounded, elongate lithified clasts of ripped-up microbial mat preserved between shallow-water stromatolitic layers in the TCG dolomite reef [Colour figure can be viewed at wileyonlinelibrary.com]

2017; Decho et al., 2005). This would explain the presence of the kerogenous films that coat the outside of the microfossiliferous and organic-rich clasts in the bedded black chert. Moreover, the two generations of silicification (i.e., within and between the clasts) suggest that the clasts may have been at least partly mineralised prior to transport and final silicification within the deeper-water environment in which they occur. Thus, perhaps when clumps of micro-organisms started to silicify, or when carbonate rhombs started to form within the colonies, these became too heavy and sunk to the seafloor to be preserved amongst the deeper-water assemblage (Decho, 2011; see also settled flocs, figure 1 in Decho & Gutierrez, 2017). The EPS films probably established whilst the clasts were suspended, or possibly after transport, but prior to lithification on the seafloor. This floating, globular colony theory better explains the range of shapes of the grainstone clasts (from round, to elongate and cuspate), and also better explains when and how the thin and delicate EPS films were able to form on the outside of clasts and yet still be preserved.

Regardless of exact process, the grainstone clasts were transported from shallower water and the microfossils within the clasts likely represent a phototrophic community. In contrast, the large, complexly branching filamentous microfossils that are preserved *in between* the kerogenous clasts could represent either a suspended or a benthic organism.

4 | CONCLUSION

Eighteen microfossil morphotypes, plus kerogenous films interpreted as EPS, are here reported as being preserved in two distinct facies of black chert from deeper-water units of the Turee Creek Group, from a ridge of outcrop located north-west of the Hardey Syncline. This ridge forms the eastern limb of the tightly folded "Kazput Syncline" (Barlow et al., 2016). Reported here are two new microfossil forms morphologically distinct from any older or younger examples known from the geological record; relatively large spherical aggregates of cells and large, complexly branching filamentous rosettes.

Separate microfossil communities are preserved in distinct nodular and bedded black chert facies, representing different environments of origin. One microfossil community, preserved in deep-water nodular black cherts interbedded with shale and ironstone, represents a primarily benthic seafloor-inhabiting community of micro-organisms that includes at least five varieties of filaments, dense unicells of one size distribution (~20 μm) and fine filamentous rosettes. Relatively large (up to ~138 μm diameter) spherical aggregate microfossils, also preserved in the nodular black chert, are likely planktonic and introduced into the deeper-water units. These spherical aggregates are unknown from the geological record and are presented here as a new microfossil form.

The other microfossil community is preserved within bedded black cherts that are interbedded with fine-grained, thinly bedded dolosiltite. In thin section, the bedded cherts consist of rounded, elongate and cuspate-shaped kerogenous clasts that are often enveloped by a thin (~2 μm) kerogenous film interpreted as preserved EPS. The clasts contain amorphous organic material and microfossils, including generally hollow unicells that are divided into three types based on size; short, degraded filaments; four types of star-shaped rosettes that commonly contain an opaque central core; and umbrella-like rosettes. Many of these forms bear resemblance to microfossils described from the shallow-water deposits of the younger (c. 1.88 Ga) Gunflint Iron Formation, including *Huroniospora*, *Eoastrion* and *K. umbellata*. Gunflint-type microbiota described here from the TCG are ~300 Ma older than the previously oldest examples of Gunflint-type microfossils from the c. 2.1 Ga Franceville Group in Gabon (Amard & Bertrand-Sarfati, 1997; Lekele Baghekema et al., 2017).

In addition, large, complexly branching filamentous microfossils are preserved between the grainstone clasts in Turee Creek Group bedded black chert units and could represent either a suspended, or benthic, organism. These are more complex and much larger than both the star-shaped rosettes and umbrella-like rosettes preserved inside the clasts, and are thus presented here as a second new microfossil form.

The grainstone clasts are interpreted as transported from shallower water, either as clasts of ripped-up microbial mat from the intertidal zone or globular colonies of floating microbial communities from near the ocean surface which, perhaps when silica or carbonate precipitation commenced, became too heavy and settled into the deeper-water setting. In either case, the microfossils from clasts in the bedded black chert studied here were once part of a shallower-water, probably phototrophic, community.

The two Turee Creek Group microfossil communities documented here provide previously unprecedented insight into the diversity of life when it would have been adjusting to the rise of atmospheric oxygen during the GOE. The fossils in the nodular black chert, interpreted as a primarily *in situ* deep-water benthic community, and those in the bedded black chert, interpreted as clasts of organic matter and microfossils transported from a shallower-water setting, provide a wide snapshot of a marine ecosystem from c. 2.4 Ga. These two distinct communities from the Turee Creek Group create a substantial new reference point in the sparse fossil record of the earliest Paleoproterozoic and highlight that microbial life at this time was more diverse than previously thought.

ACKNOWLEDGMENTS

Many thanks to J. Jesse, B. Nomchong and G. Soares for field assistance; M. R. Walter and T. Djokic for insightful discussions; J. Wilde and J. Duggan for thin section preparation; and R. Buick and three anonymous reviewers for comments and suggestions that helped to improve this manuscript. Research support was provided by the Australian Centre for Astrobiology and School of Biological, Earth and Environmental Sciences at the University of New South Wales, and the Australian Research Council Centre of Excellence for Core to

Crust Fluid Systems. EVB also received support through an Australian Government Research Training Program Scholarship.

CONFLICT OF INTEREST

The authors declare no conflict of interest.

ORCID

Erica Victoria Barlow http://orcid.org/0000-0001-6234-1343

REFERENCES

Amard, B., & Bertrand-Sarfati, J. (1997). Microfossils in 2000 Ma old cherty stromatolites of the Franceville Group, Gabon. *Precambrian Research*, *81*, 197–221. https://doi.org/10.1016/S0301-9268(96)00035-6

Awramik, S. M. (1976). Gunflint stromatolites: Microfossil distribution in relation to stromatolite morphology. In M. R. Walter (Ed.), *Stromatolites. Developments in sedimentology, No. 20* (pp. 311–320). Amsterdam, The Netherlands: Elsevier.

Awramik, S. M., & Barghoorn, E. S. (1977). The Gunflint microbiota. *Precambrian Research*, *5*, 121–142. https://doi.org/10.1016/0301-9268(77)90025-0

Barghoorn, E. S., & Tyler, S. A. (1965). Microorganisms from the Gunflint chert. *Science*, *147*, 563–575. https://doi.org/10.1126/science.147.3658.563

Barley, M. E., Pickard, A. L., & Sylvester, P. J. (1997). Emplacement of a large igneous province as a possible cause of banded iron formation 2.45 billion years ago. *Nature*, *385*, 55–58. https://doi.org/10.1038/385055a0

Barlow, E., Van Kranendonk, M. J., Yamaguchi, K. E., Ikehara, M., & Lepland, A. (2016). Lithostratigraphic analysis of a new stromatolite-thrombolite reef from across the rise of atmospheric oxygen in the Paleoproterozoic Turee Creek Group, Western Australia. *Geobiology*, *14*, 317–343. https://doi.org/10.1111/gbi.12175

Bartley, J. K. (1996). Actualistic taphonomy of cyanobacteria: implications for the Precambrian fossil record. *Palaios*, *11*, 571–586. https://doi.org/10.2307/3515192

Bekker, A., Holland, H. D., Wang, P.-L., Rumble, D., Stein, H. J., Hannah, J. L., … Beukes, N. J. (2004). Dating the rise of atmospheric oxygen. *Nature*, *427*, 117–120. https://doi.org/10.1038/nature02260

Berelson, W. M., Corsetti, F. A., Pepe-Ranney, C., Hammond, D. E., Beaumont, W., & Spear, J. R. (2011). Hot spring siliceous stromatolites from Yellowstone National Park: Assessing growth rate and laminae formation. *Geobiology*, *9*, 411–424.

Boggs, S. (2009). *Petrology of sedimentary rocks* (p. 600). New York, NY: Cambridge University Press. https://doi.org/10.1017/CBO9780511626487

Butterfield, N. J. (2001). Paleobiology of the late Mesoproterozoic (ca. 1200 Ma) hunting formation, Somerset Island, arctic Canada. *Precambrian Research*, *111*, 235–256. https://doi.org/10.1016/S0301-9268(01)00162-0

Butterfield, N. J. (2005a). Probable proterozoic fungi. *Paleobiology*, *31*, 165–182. https://doi.org/10.1666/0094-8373(2005)031<0165:PPF>2.0.CO;2

Butterfield, N. J. (2005b). Reconstructing a complex early Neoproterozoic eukaryote, Wynniatt Formation, arctic Canada. *Lethaia*, *38*, 155–169. https://doi.org/10.1080/00241160510013231

Butterfield, N. J., Knoll, A. H., & Swett, K. (1990). A bangiophyte red alga from the Proterozoic of arctic Canada. *Science*, *250*, 104–108. https://doi.org/10.1126/science.11538072

Chowns, T. M., & Elkins, J. E. (1974). The origin of quartz geodes and cauliflower cherts through the silicification of anhydrite nodules. *Journal of Sedimentary Petrology*, *44*, 885–903.

Cloud, P. E. (1965). Significance of the Gunflint (Precambrian) microflora. Photosynthetic oxygen may have had important local effects before becoming a major atmospheric gas. *Science*, *148*, 27–35. https://doi.org/10.1126/science.148.3666.27

Cloud, P. (1976). Beginnings of biospheric evolution and their biogeochemical consequences. *Paleobiology*, *2*, 351–387. https://doi.org/10.1017/S009483730000498X

Cloud, P., & Morrison, K. (1980). New microbial fossils from 2 Gyr old rocks in northern Michigan. *Geomicrobiology Journal*, *2*, 161–178. https://doi.org/10.1080/01490458009377759

Czaja, A. D., Beukes, N. J., & Osterhout, J. T. (2016). Sulfur-oxidizing bacteria prior to the Great Oxidation Event from the 2.52 Ga Gamohaan Formation of South Africa. *Geology*, *44*, 983–986. https://doi.org/10.1130/G38150.1

Decho, A. W. (2011). Extracellular polymeric substances (EPS). In J. Reitner, & V. Theil (Eds.), *Encyclopedia of geobiology* (pp. 359–361). Dordrecht, The Netherlands: Springer. https://doi.org/10.1007/978-1-4020-9212-1

Decho, A. W., & Gutierrez, T. (2017). Microbial extracellular polymeric substances (EPSs) in ocean systems. *Frontiers in Microbiology*, *8*, 922. https://doi.org/10.3389/fmicb.2017.00922

Decho, A. W., Visscher, P. T., & Reid, R. (2005). Production and cycling of natural microbial exopolymers (EPS) within a marine stromatolite. *Palaeogeography, Palaeoclimatology, Palaeoecology*, *219*, 71–86. https://doi.org/10.1016/j.palaeo.2004.10.015

Dupraz, C., Fowler, A., Tobias, C., & Visscher, P. T. (2013). Stromatolitic knobs in Storr's Lake (San Salvador, Bahamas): A model system for formation and alteration of laminae. *Geobiology*, *11*, 527–548. https://doi.org/10.1111/gbi.12063

Fadel, A., Lepot, K., Busigny, V., Addad, A., & Troadec, D. (2017). Iron mineralisation and taphonomy of microfossils of the 2.45-2.21 Ga Turee Creek Group, Western Australia. *Precambrian Research*, *298*, 530–551. https://doi.org/10.1016/j.precamres.2017.07.003

Farquhar, J., Bao, H., & Thiemens, M. (2000). Atmospheric influence of Earth's earliest sulfur cycle. *Science*, *289*, 756–758. https://doi.org/10.1126/science.289.5480.756

Flemming, H. C., & Wingender, J. (2001). Relevance of microbial extracellular polymeric substances (EPSs) – Part I: Structural and ecological aspects. *Water Science and Technology*, *43*, 1–8. https://doi.org/10.2166/wst.2001.0326

Flemming, H. C., & Wingender, J. (2010). The biofilm matrix. *Nature Reviews Microbiology*, *8*, 623–633. https://doi.org/10.1038/nrmicro2415

Flugel, E. (2004). *Microfacies of carbonate rocks: Analysis, interpretation and application* (p. 996). Berlin Heidelberg, Germany: Springer. https://doi.org/10.1007/978-3-662-08726-8

Fowler, A. J. (2011). *Stromatolitic knobs in storrs lake, san salvador, bahamas: Insights into organomineralization*. Masters Thesis, 180 p. http://digitalcommons.uconn.edu/gs_theses/180

Fralick, P., Davis, D. W., & Kissin, S. A. (2002). The age of the Gunflint Formation, Ontario, Canada: Single zircon U Pb age determinations from reworked volcanic ash. *Canadian Journal of Earth Sciences*, *39*, 1085–1091. https://doi.org/10.1139/e02-028

Geological Survey of Western Australia (2017). *Extracted from GeoVIEW. WA on 01/04/2017* Perth, Western Australia: Department of Mines and Petroleum.

Golubic, S., & Hofmann, H. J. (1976). Comparison of Holocene and mid-Precambrian Entophysalidaceae (Cyanophyta) in stromatolitic algal mats: Cell division and degradation. *Journal of Paleontology*, *50*, 1074–1082.

Grey, K. (1985). Stromatolites in the Proterozoic Duck Creek Dolomite, Western Australia. *Geological Survey of Western Australia*, *14*, 94–103.

Grey, K., & Thorne, A. M. (1985). Biostratigraphic significance of stromatolites in upward shallowing sequences of the early Proterozoic Duck Creek Dolomite, Western Australia. *Precambrian Research*, *29*, 183–206. https://doi.org/10.1016/0301-9268(85)90068-3

Grotzinger, J. P., & Knoll, A. H. (1999). Stromatolites in Precambrian carbonates: Evolutionary mileposts or environmental dipsticks? *Annual Review of Earth and Planetary Sciences*, *27*, 313–358. https://doi.org/10.1146/annurev.earth.27.1.313

Helm, R. F., & Potts, M. (2012). Extracellular matrix (ECM). In B. A. Whitton (Ed.), *Ecology of cyanobacteria II: Their diversity in space and time* (pp. 461–480). Dordrecht, The Netherlands: Springer. https://doi.org/10.1007/978-94-007-3855-3

Hickman, A. H., & Van Kranendonk, M. J. (2012). *A billion years of earth history: A geological transect through the pilbara craton and the mount Bruce supergroup – a field guide to accompany 34th IGC Excursion WA-2*. Geological Survey of Western Australia Record 2012/10, 66 p.

Hofmann, H. J. (1976). Precambrian microflora, Belcher Islands, Canada: Significance and systematics. *Journal of Paleontology*, *50*, 1040–1073.

Holland, H. D. (2002). Volcanic gases, black smokers, and the Great Oxidation Event. *Geochimica et Cosmochimica Acta*, *66*, 3811–3826. https://doi.org/10.1016/S0016-7037(02)00950-X

Javaux, E. J., & Knoll, A. H. (2016). Micropaleontology of the lower Mesoproterozoic Roper Group, Australia, and implications for early eukaryotic evolution. *Journal of Paleontology*, *91*, 199–229.

Klaveness, D. (1977). Morphology, distribution and significance of the manganese-accumulating microorganism *Metallogenium* in lakes. *Hydrobiologia*, *56*, 25–33. https://doi.org/10.1007/BF00023282

Klaveness, D. (1999). *Metallogenium* – A microbial enigma. In J. Seckbach (Ed.), *Enigmatic microorganisms and life in extreme environments* (pp. 539–548). Dordrecht, The Netherlands: Springer. https://doi.org/10.1007/978-94-011-4838-2

Klein, C., Beukes, N. J., & Schopf, J. W. (1987). Filamentous microfossils in the early Proterozoic Transvaal Supergroup: Their morphology, significance, and paleoenvironmental setting. *Precambrian Research*, *36*, 81–94. https://doi.org/10.1016/0301-9268(87)90018-0

Knoll, A. H., & Barghoorn, E. S. (1976). A gunflint-type microbiota from the Duck Creek Dolomite, Western Australia. *Origins of Life*, *7*, 417–423. https://doi.org/10.1007/BF00927937

Knoll, A. H., & Barghoorn, E. S. (1977). Archean microfossils showing cell division from the Swaziland System of South Africa. *Science*, *198*, 396–398. https://doi.org/10.1126/science.198.4315.396

Knoll, A. H., Barghoorn, E. S., & Awramik, S. M. (1978). New microorganisms from the Aphebian Gunflint Iron Formation, Ontario. *Journal of Paleontology*, *52*, 976–992.

Knoll, A. H., & Simonson, B. (1981). Early Proterozoic microfossils and penecontemporaneous quartz cementation in the Sokoman Iron Formation, Canada. *Science*, *211*, 478–480. https://doi.org/10.1126/science.211.4481.478

Knoll, A. H., Strother, P. K., & Rossi, S. (1988). Distribution and diagenesis of microfossils from the lower Proterozoic Duck Creek Dolomite, Western Australia. *Precambrian Research*, *38*, 257–279. https://doi.org/10.1016/0301-9268(88)90005-8

Konhauser, K. O., Phoenix, V. R., Bottrell, S. H., Adams, D. G., & Head, I. M. (2001). Microbial-silica interactions in Icelandic hot spring sinter: Possible analogues for some Precambrian siliceous stromatolites. *Sedimentology*, *48*, 415–433. https://doi.org/10.1046/j.1365-3091.2001.00372.x

Krapez, B. (1996). Sequence stratigraphic concepts applied to the identification of basin-filling rhythms in Precambrian successions. *Australian Journal of Earth Sciences*, *43*, 355–380. https://doi.org/10.1080/08120099608728260

Krapez, B. (1999). Stratigraphic record of an Atlantic-type global tectonic cycle in the Palaeoproterozoic Ashburton Province of Western Australia. *Australian Journal of Earth Sciences*, *46*, 71–87. https://doi.org/10.1046/j.1440-0952.1999.00688.x

Krapez, B., Müller, S. G., Fletcher, I. R., & Rasmussen, B. (2017). A tale of two basins? Stratigraphy and detrital zircon provenance of the Palaeoproterozoic Turee Creek and Horseshoe basins of Western Australia. *Precambrian Research*, *294*, 67–90. https://doi.org/10.1016/j.precamres.2017.03.020

Kremer, B., & Kazmierczak, J. (2017). Cellularly preserved microbial fossils from ~3.4 Ga deposits of South Africa: A testimony of early appearance of oxygenic life? *Precambrian Research*, *295*, 117–129. https://doi.org/10.1016/j.precamres.2017.04.023

Lan, Z. W., Li, X., Chen, Z. Q., Li, Q., Hofmann, A., Zhang, Y., … Li, J. (2014). Diagenetic xenotime age constraints on the Sanjiaotang Formation, Luoyu Group, southern margin of the North China Craton: Implications for regional stratigraphic correlation and early evolution of eukaryotes. *Precambrian Research*, *251*, 21–32. https://doi.org/10.1016/j.precamres.2014.06.012

Lanier, W. P. (1986). Approximate growth rates of Early Proterozoic microstromatolites as deduced by biomass productivity. *Palaios*, *1*, 525–542. https://doi.org/10.2307/3514705

Lanier, W. P. (1989). Interstitial and peloid microfossils from the 2.0 Ga Gunflint Formation: Implications for the paleoecology of the Gunflint stromatolites. *Precambrian Research*, *45*, 291–318. https://doi.org/10.1016/0301-9268(89)90067-3

Lekele Baghekema, S. G., Lepot, K., Riboulleau, A., Fadel, A., Trentesaux, A., & El Albani, A. (2017). Nanoscale analysis of preservation of ca. 2.1 Ga old Francevillian microfossils, Gabon. *Precambrian Research*, *301*, 1–18.

Lepot, K., Addad, A., Knoll, A. H., Wang, J., Troadec, D., Béché, A., & Javaux, E. J. (2017). Iron minerals within specific microfossil morphospecies of the 1.88 Ga Gunflint Formation. *Nature Communications*, *8*, 14890. https://doi.org/10.1038/ncomms14890

Maliva, R. G., Knoll, A. H., & Simonson, B. M. (2005). Secular changes in the Precambrian silica cycle: Insights from chert petrology. *Geological Society of America Bulletin*, *117*, 835–845. https://doi.org/10.1130/B25555.1

Martin, D. M. (1999). Depositional setting and implications of Paleoproterozoic glaciomarine sedimentation in the Hamersley Province, Western Australia. *Geological Society of America Bulletin*, *111*, 189–203. https://doi.org/10.1130/0016-7606(1999)111<0189:DSAIOP>2.3.CO;2

Martin, D. M., Li, Z. X., Nemchin, A. A., & Powell, C. M. (1998). A pre-2.2 Ga age for giant hematite ores of the Hamersley Province, Australia? *Economic Geology*, *93*, 1084–1090. https://doi.org/10.2113/gsecongeo.93.7.1084

Martin, D. M. c. B., & Morris, P. A. (2010). Tectonic setting and regional implications of ca 2.2 Ga mafic magmatism in the southern Hamersley Province, Western Australia. *Australian Journal of Earth Sciences*, *57*, 911–931. https://doi.org/10.1080/08120099.2010.510172

Martin, D. M. c. B., Powell, C. M. c. A., & George, A. D. (2000). Stratigraphic architecture and evolution of the early Paleoproterozoic McGrath Trough, Western Australia. *Precambrian Research*, *99*, 33–64. https://doi.org/10.1016/S0301-9268(99)00053-4

Mata, S. A., Harwood, C. L., Corsetti, F. A., Stork, N. J., Eilers, K., Berelson, W. M., & Spear, J. R. (2012). Influence of gas production and filament orientation on stromatolite microfabric. *Palaios*, *27*, 206–219. https://doi.org/10.2110/palo.2011.p11-088r

Milliken, K. L. (1979). The silicified evaporite syndrome – Two aspects of the silicification history of former evaporate nodules from southern Kentucky and northern Tennessee. *Journal of Sedimentary Petrology*, *49*, 245–256.

Monty, C. L. V. (1967). Recent algal stromatolitic deposits, Andros Island, Bahamas: Preliminary Report. *Geologische Rundschau*, *61*, 742–783.

Monty, C. L. V. (1976). The origin and development of cryptalgal fabrics. In M. R. Walter (Ed.), *Stromatolites. Developments in sedimentology, No. 20* (pp. 193–249). Amsterdam, The Netherlands: Elsevier.

Nielsen, L. P., Risgaard-Petersen, N., Fossing, H., Christensen, P. B., & Sayama, M. (2010). Electric currents couple spatially separated

biogeochemical processes in marine sediment. *Nature*, *463*, 1071–1074. https://doi.org/10.1038/nature08790

Oehler, D. Z. (1976a). Transmission electron microscopy of organic microfossils from the late Precambrian Bitter Springs Formation of Australia: Techniques and survey of preserved ultrastructure. *Journal of Paleontology*, *50*, 90–106.

Oehler, J. H. (1976b). Hydrothermal crystallization of silica gel. *Geological Society of America Bulletin*, *87*, 1143–1152. https://doi.org/10.1130/0016-7606(1976)87<1143:HCOSG>2.0.CO;2

Oehler, J. H. (1977). Microflora of the HYC pyritic shale member of the Barney Creek Formation (McArthur Group), middle Proterozoic of northern Australia. *Alcheringa*, *1*, 315–349. https://doi.org/10.1080/03115517708527768

Peat, C. J., Muir, M. D., Plumb, K. A., McKirdy, D. M., & Norvick, M. S. (1978). Proterozoic microfossils from the Roper Group, Northern Territory, Australia. *BMR Journal of Australian Geology and Geophysics*, *3*, 1–17.

Pfeffer, C., Larsen, S., Song, J., Dong, M., Besenbacher, F., Meyer, R. L., … Nielsen, L. P. (2012). Filamentous bacteria transport electrons over centimetre distances. *Nature*, *491*, 218–221. https://doi.org/10.1038/nature11586

Porter, S. M., Meisterfeld, R., & Knoll, A. H. (2003). Vase-shaped microfossils from the Neoproterozoic Chuar Group, Grand Canyon: A classification guided by modern testate amoebae. *Journal of Paleontology*, *77*, 409–429. https://doi.org/10.1017/S0022336000044140

Powell, C. M. C. A., & Horwitz, R. C. (1994). Late Archaean and early Proterozoic tectonics and basin formation of the Hamersley ranges. *Geological Society of Australia (WA Division) Excursion Guidebook 4*, 57 p.

Ramsing, N. B., Ferris, M. J., & Ward, D. M. (2000). Highly ordered vertical structure of Synechococcus populations within the one-millimeter-thick photic zone of a hot spring cyanobacterial mat. *Applied and Environmental Microbiology*, *66*, 1038–1049. https://doi.org/10.1128/AEM.66.3.1038-1049.2000

Reitner, J. (2011). *Metallogenium*. In J. Reitner, & V. Thiel (Eds.), *Encyclopedia of geobiology* (pp. 563–564). Dordrecht, The Netherlands: Springer. https://doi.org/10.1007/978-1-4020-9212-1

Riley, G. A. (1963). Organic aggregates in seawater and the dynamics of their formation and utilization. *Limnology and Oceanography*, *8*, 372–381. https://doi.org/10.4319/lo.1963.8.4.0372

Riley, G. A. (1970). Particulate organic matter in sea water. *Advances in Marine Biology*, *8*, 1–118.

Riley, G. A., Van Hemart, D., & Wangersky, P. J. (1965). Organic aggregates in surface and deep waters of the Sargasso Sea. *Limnology and Oceanography*, *10*, 354–363. https://doi.org/10.4319/lo.1965.10.3.0354

Riley, G. A., Wanngersky, P. J., & Van Hemart, D. (1964). Organic aggregates in tropical and subtropical surface waters of the North Atlantic Ocean. *Limnology and Oceanography*, *9*, 546–550. https://doi.org/10.4319/lo.1964.9.4.0546

Ruff, S. W., & Farmer, J. D. (2016). Silica deposits on Mars with features resembling hot spring biosignatures at El Tatio in Chile. *Nature Communications*, *7*, 13554. https://doi.org/10.1038/ncomms13554

Schopf, J. W., Kudryavtsev, A. B., Czaja, A. D., & Tripathi, A. B. (2007). Evidence of Archean life: Stromatolites and microfossils. *Precambrian Research*, *158*, 141–155. https://doi.org/10.1016/j.precamres.2007.04.009

Schopf, J. W., Kudryavtsev, A. B., Walter, M. R., Van Kranendonk, M. J., Williford, K. H., Kozdon, R., … Flannery, D. T. (2015). Sulfur-cycling fossil bacteria from the 1.8-Ga Duck Creek Formation provide promising evidence of evolution's null hypothesis. *Proceedings of the National Academy of Sciences*, *112*, 2087–2092. https://doi.org/10.1073/pnas.1419241112

Schulz, H. N., & Jorgensen, B. B. (2001). Big bacteria. *Annual Reviews Microbiology*, *55*, 105–137. https://doi.org/10.1146/annurev.micro.55.1.105

Schulz, H. N., Jorgensen, B. B., Fossing, H. A., & Ramsing, N. B. (1996). Community structure of filamentous, sheath-building sulfur bacteria, *Thioploca* spp., off the coast of Chile. *Applied and Environmental Microbiology*, *62*, 1855–1862.

Siever, R. (1957). The silica budget in the sedimentary cycle. *American Mineralogist*, *42*, 821–841.

Siever, R. (1992). The silica cycle in the Precambrian. *Geochimica et Cosmochimica Acta*, *56*, 3265–3272. https://doi.org/10.1016/0016-7037(92)90303-Z

Simonson, B. M., Schubel, K. A., & Hassler, S. W. (1993). Carbonate sedimentology of the early Precambrian Hamersley Group of Western Australia. *Precambrian Research*, *60*, 287–335. https://doi.org/10.1016/0301-9268(93)90052-4

Sugitani, K., Grey, K., Allwood, A., Nagaoka, T., Mimura, K., Minami, M., … Walter, M. R. (2007). Diverse microstructures from Archaean chert from the Mount Goldsworthy-Mount Grant area, Pilbara Craton, Western Australia: Microfossils, dubiofossils, or pseudofossils? *Precambrian Research*, *158*, 228–262. https://doi.org/10.1016/j.precamres.2007.03.006

Sugitani, K., Grey, K., Nagaoka, T., Mimura, K., & Walter, M. R. (2009). Taxonomy and biogenicity of Archaean spheroidal microfossils (ca. 3.0 Ga) from the Mount Goldsworthy-Mount Grant area in the northeastern Pilbara Craton, Western Australia. *Precambrian Research*, *173*, 50–59. https://doi.org/10.1016/j.precamres.2009.02.004

Sugitani, K., Lepot, K., Nagaoka, T., Mimura, K., Van Kranendonk, M. J., Oehler, D. Z., & Walter, M. R. (2010). Biogenicity of morphologically diverse carbonaceous microstructures from the ca. 3400 Ma Strelley Pool Formation, in the Pilbara Craton, Western Australia. *Astrobiology*, *10*, 899–920. https://doi.org/10.1089/ast.2010.0513

Sugitani, K., Mimura, K., Nagaoka, T., Lepot, K., & Takeuchi, M. (2013). Microfossil assemblage from the 3400 Ma Strelley Pool Formation in the Pilbara Craton, Western Australia: Results form a new locality. *Precambrian Research*, *226*, 59–74. https://doi.org/10.1016/j.precamres.2012.11.005

Sugitani, K., Mimura, K., Takeuchi, M., Lepot, K., Ito, S., & Javaux, E. J. (2015). Early evolution of large micro-organisms with cytological complexity revealed by microanalyses of 3.4 Ga organic-walled microfossils. *Geobiology*, *13*, 507–521. https://doi.org/10.1111/gbi.12148

Sugitani, K., Mimura, K., Takeuchi, M., Yamaguchi, T., Suzuki, K., Senda, R., … Van Kranendonk, M. J. (2015). A Paleoarchean coastal hydrothermal field inhabited by diverse microbial communities: The Strelley Pool Formation, Pilbara Craton, Western Australia. *Geobiology*, *13*, 522–545. https://doi.org/10.1111/gbi.12150

Thorne, A. M., & Tyler, I. M. (1996). *Geology of the Rocklea 1:100 000 sheet*. Geological Survey of Western Australia, 1:100 000 Series – Explanatory Notes.

Thorne, A. M., Tyler, I. M., & Blight, D. F. (1995). *Rocklea, W.A., geological survey of Western Australia, 1:100 000 geological series*.

Tobin, K. J. (1990). The paleoecology and significance of the Gunflint-type microbial assemblages from the Frere Formation (Early Proterozoic), Nabberu Basin, Western Australia. *Precambrian Research*, *47*, 71–81. https://doi.org/10.1016/0301-9268(90)90031-K

Trendall, A. F. (1979). A revision of the Mount Bruce Supergroup. *Geological Survey of Western Australia Annual Report*, *1978*, 63–71.

Trendall, A. F., Compston, W., Nelson, D. R., De Laeter, J. R., & Bennett, V. C. (2004). SHRIMP zircon ages constraining the depositional chronology of the Hamersley Group, Western Australia. *Australian Journal of Earth Sciences*, *51*, 621–644. https://doi.org/10.1111/j.1400-0952.2004.01082.x

Turner, E. C., James, N. P., & Narbonne, G. M. (2000). Taphonomic control on microstructure in Early Neoproterozoic reefal stromatolites and thrombolites. *Palaios*, *15*, 87–111. https://doi.org/10.1669/0883-1351(2000)015<0087:TCOMIE>2.0.CO;2

Tyler, S. A., & Barghoorn, E. S. (1954). Occurrence of structurally preserved plants in pre-Cambrian rocks of the Canadian Shield. *Science*, *119*, 606–608. https://doi.org/10.1126/science.119.3096.606

Van Kranendonk, M. J. (2010). *Three and a half billion years of life on Earth: A transect back into deep time*. Geological Survey of Western Australia, Record 2010/21, 93 p.

Van Kranendonk, M. J., Mazumder, R., Yamaguchi, K. E., Yamada, K., & Ikehara, M. (2015). Sedimentology of the Paleoproterozoic Kungarra Formation, Turee Creek Group, Western Australia: A conformable record of the transition from early to modern Earth. *Precambrian Research*, *256*, 314–343. https://doi.org/10.1016/j.precamres.2014.09.015

Van Kranendonk, M. J., Schopf, J. W., Grice, K., Walter, M. R, Pages, A., Kudryavtsev, A. B., … Lepland, A. (2012). A 2.3 Ga sulfuretum at the GOE: Microfossils and organic geochemistry evidence from the Turee Creek Group, Western Australia. In: *Astrobiology science conference abstract*. Atlanta, GA, USA.

Wacey, D., Kilburn, M. R., Saunders, M., Cliff, J., & Brasier, M. D. (2011). Microfossils of sulphur-metabolizing cells in 3.4-billion-year-old rocks of Western Australia. *Nature Geoscience*, *4*, 698–702. https://doi.org/10.1038/ngeo1238

Wacey, D., Menon, S., Green, L., Gerstmann, D., Kong, C., Mcloughlin, N., … Brasier, M. (2012). Taphonomy of very ancient microfossils from the ~3400 Ma Strelley Pool Formation and ~1900 Ma Gunflint Formation: New insights using a focused ion beam. *Precambrian Research*, *220–221*, 234–250. https://doi.org/10.1016/j.precamres.2012.08.005

Wagstaff, K. L., & Corsetti, F. A. (2010). An evaluation of information-theoretic methods for detecting structural microbial biosignatures. *Astrobiology*, *10*, 363–379. https://doi.org/10.1089/ast.2008.0301

Walsh, M. M. (1992). Microfossils and possible microfossils from the Early Archean Onverwacht Group, Barberton Mountain Land, South Africa. *Precambrian Research*, *54*, 271–293. https://doi.org/10.1016/0301-9268(92)90074-X

Walsh, M. M., & Lowe, D. R. (1985). Filamentous microfossils from the 3,500-Myr-old Onverwacht Group, Barberton Mountain Land, South Africa. *Nature*, *314*, 530–532. https://doi.org/10.1038/314530a0

Walsh, M. M., & Lowe, D. R. (1999). Modes of accumulation of carbonaceous matter in the early Archean: A petrographic and geochemical study of the carbonaceous cherts of the Swaziland Supergroup. In D. R. Lowe, & G. R. Byerly (Eds.), *Geologic evolution of the Barberton greenstone belt, South Africa* (pp. 115–132). Geological Society of America Special Paper Vol. 329, Boulder CO. https://doi.org/10.1007/978-3-662-13187-9

Walter, M. R. (1972). Stromatolites and the biostratigraphy of the Australian Precambrian and Cambrian. *Special Papers in Paleontology*, *11*, 256.

Walter, M. R. (1976). *Stromatolites*. *Developments in sedimentology*, *No. 20* (p. 790). Amsterdam, The Netherlands: Elsevier.

Williford, K. H., Van Kranendonk, M. J., Ushikubo, T., Kozdon, R., & Valley, J. W. (2011). Constraining atmospheric oxygen and seawater sulfate concentrations during Paleoproterozoic glaciation: In situ sulfur three-isotope microanalysis of pyrite from the Turee Creek Group, Western Australia. *Geochimica et Cosmochimica Acta*, *75*, 5686–5705. https://doi.org/10.1016/j.gca.2011.07.010

Wilson, J. P., Fischer, W. W., Johnston, D. T., Knoll, A. H., Grotzinger, J. P., Walter, M. R., … Watters, W. (2010). Geobiology of the late Paleoproterozoic Duck Creek Formation, Western Australia. *Precambrian Research*, *179*, 135–149. https://doi.org/10.1016/j.precamres.2010.02.019

Xiao, S., Schiffbauer, J. D., McFadden, K. A., & Hunter, J. (2010). Petrographic and SIMS pyrite sulfur isotope analyses of Ediacaran chert nodules: Implications for microbial processes in pyrite rim formation, silicification, and exceptional fossil preservation. *Earth and Planetary Science Letters*, *297*, 481–495. https://doi.org/10.1016/j.epsl.2010.07.001

Yin, L. (1997). Acanthomorphic acritarchs from Meso-Neoproterozoic shales of the Ruyang Group, Shanxi, China. *Review of Palaeobotany and Palynology*, *98*, 15–25. https://doi.org/10.1016/S0034-6667(97)00022-5

Yin, L., Xunlai, Y., Fanwei, M., & Jie, H. (2005). Protists of the upper Mesoproterozoic Ruyang Group in Shanxi Province, China. *Precambrian Research*, *141*, 49–66.

Zavarzin, G. A. (1981). The genus *Metallogenium*. In M. P. Starr, H. Stolp, H. B. Trueper, A. Balows, & H. G. Schlegel (Eds.), *The prokaryotes* (pp. 524–528). Berlin, Germany: Springer.

SUPPORTING INFORMATION

Additional supporting information may be found online in the Supporting Information section at the end of the article.

How to cite this article: Barlow EV, Van Kranendonk MJ. Snapshot of an early Paleoproterozoic ecosystem: Two diverse microfossil communities from the Turee Creek Group, Western Australia. *Geobiology*. 2018;16:449–475. https://doi.org/10.1111/gbi.12304